DOI: 10.1021/ic902314f

Inorganic Chemistry
Article

Planned Failures from the Principle of Maximum Site Occupancy in Lanthanide Helicates

Jean-François Lemonnier,*,† Laure Guénée,*,† Gérald Bernardinelli,‡ Jean-François Vigier,†,§ Bernard Bocquet,† and Claude Piguet*,†

†*Department of Inorganic, Analytical and Applied Chemistry, University of Geneva, 30 quai E. Ansermet, CH-1211 Geneva 4, Switzerland and* ‡*Laboratory of Crystallography, University of Geneva, 24 quai E. Ansermet, CH-1211 Geneva 4, Switzerland.* §*Current address: Cité Scientifique, Bat. C7, Avenue Mendeleïev, BP 90108, F-59652 Villeneuve d'Ascq Cedex, France.*

Received November 23, 2009

Despite the recent emergence of a toolbox fitted with microscopic thermodynamic descriptors for predicting the stabilities and speciations of polynuclear complexes in solution, the discovery of novel or unusual type of metal−ligand assemblies in metallosupramolecular chemistry still often relies on serendipity. In order to highlight the novel perspectives offered by a rational exploitation of these thermodynamic parameters, the segmental bis-tridentate ligands **L7** and **L8** have been designed for providing effective molarities upon reaction with trivalent lanthanides, Ln(III), so small that the saturated binuclear triple-stranded helicates $[Ln_2(\mathbf{Lk})_3]^{6+}$, which obey the well-respected principle of maximum site occupancy, cannot be detected in solution because of their deliberately planned instabilities. The hierarchical evolution of the effective molarities with an increasing number of ligand strands in these complexes indeed favors the formation of the alternative unsaturated single-stranded $[Ln_2(\mathbf{Lk})]^{6+}$ and double-stranded $[Ln_2(\mathbf{Lk})_2]^{6+}$ complexes, whose relative speciations in solution depend on the nature of the binding sites introduced into the segmental ligand.

Introduction

It is now well-established that the cumulative stability constant of any self-assembly process involving metals and ligands (equilibrium 1) can be modeled with the simple free energy additive strategy shown in eq 2.[1]

$$m\mathrm{M}^{z+} + n\mathrm{L} \rightleftharpoons [\mathrm{M}_m\mathrm{L}_n]^{mz+} \quad \beta_{m,n}^{\mathrm{M,L}} \tag{1}$$

$$\beta_{m,n}^{\mathrm{M,L}} = \omega_{\mathrm{chir}}^{\mathrm{M,L}} \cdot \omega_{m,n}^{\mathrm{M,L}} \cdot \prod_{i=1}^{m\cdot n} (f_i^{\mathrm{M,L}}) \cdot \prod_{i=1}^{m\cdot n-m-n+1} (c_i^{\mathrm{eff}}) \cdot \prod_{k}^{''} (u_k^{\mathrm{M,M}}) \cdot \prod_{l}^{'''} (u_l^{\mathrm{L,L}}) \tag{2}$$

$\omega_{\mathrm{chir}}^{\mathrm{M,L}} \cdot \omega_{m,n}^{\mathrm{M,L}}$ is the statistical factor of the assembly,[2] $f_i^{\mathrm{M,L}}$ is the hetero-component intermolecular microscopic affinity characterizing the connection of a metal M to the binding site *i* of a ligand L (including desolvation), c^{eff} is the effective concentration correcting $f_i^{\mathrm{M,L}}$ for intramolecular macrocyclization complexation processes,[3] and $u_k^{\mathrm{M,M}} = \exp(-\Delta E_k^{\mathrm{M,M}}/RT)$ and $u_l^{\mathrm{L,L}} = \exp(-\Delta E_l^{\mathrm{L,L}}/RT)$ are the Boltzmann factors accounting for the homo-component intermetallic $\Delta E_k^{\mathrm{M,M}}$ and interligand $\Delta E_l^{\mathrm{L,L}}$ interactions.[4] Classical coordination chemistry mainly relies on the deliberate design of favorable intermolecular metal−ligand interactions, which overcome desolvation processes ($f_i^{\mathrm{M,L}} > 0$) and thus produce negative contributions to the free energy changes accompanying the complexation process: i.e., $\Delta G_{\mathrm{inter}}^{\mathrm{M,L}} = -RT \ln(f_i^{\mathrm{M,L}}) < 0$. Consequently, the minimization of the global free energy change $\Delta G_{m,n}^{\mathrm{M,L}} = -RT \ln(\beta_{m,n}^{\mathrm{M,L}})$,[5] which is responsible for the

*To whom correspondence should be addressed. E-mail: Claude.Piguet@unige.ch (C.P.); Jean.Lemonnier@unige.ch (J.-F.L.); Laure.Guenee@unige.ch (L.G.).

(1) (a) Hamacek, J.; Borkovec, M.; Piguet, C. *Dalton Trans.* **2006**, 1473–1490. (b) Fyles, T. M.; Tong, C. C. *New J. Chem.* **2007**, *31*, 296–304.

(2) Ercolani, G.; Piguet, C.; Borkovec, M.; Hamacek, J. *J. Phys. Chem. B* **2007**, *111*, 12195−12203 and references therein.

(3) (a) Kuhn, W. *Kolloid Z.* **1934**, *68*, 2–15. (b) Jacobson, H.; Stockmayer, W. H. *J. Chem. Phys.* **1950**, *18*, 1600–1606. (c) Flory, P. J.; Suter, U. W.; Mutter, M. *J. Am. Chem. Soc.* **1976**, *98*, 5733–5739. (d) Jencks, W. P. *Proc. Natl. Acad. Sci. U.S.A.* **1981**, *78*, 4046–4050. (e) Winnik, M. A. *Chem. Rev.* **1981**, *81*, 491–524. (f) Mandolini, L. *Adv. Phys. Org. Chem.* **1986**, *22*, 1–111. (g) Chi, X.; Guerin, A. J.; Haycock, R. A.; Hunter, C. A.; Sarson, L. D *J. Chem. Soc., Chem. Commun.* **1995**, 2563–2654. (h) Ercolani, G. *J. Phys. Chem. B* **1998**, *102*, 5699–5703. (i) Kramer, R. H.; Karpen, J. W. *Nature* **1998**, *395*, 710–713. (j) Galli, C.; Mandolini, L. *Eur. J. Org. Chem.* **2000**, 3117–3125. (k) Gargano, J. M.; Ngo, T.; Kim, J. Y.; Acheson, D. W. K.; Lees, W. J. *J. Am. Chem. Soc.* **2001**, *123*, 12909–12910. (l) Kitov, P. I.; Bundle, D. R. *J. Am. Chem. Soc.* **2003**, *125*, 16271–16284.

(4) (a) Canard, G.; Piguet, C. *Inorg. Chem.* **2007**, *46*, 3511–3522. (b) Borkovec, M.; Koper, G. J. M.; Piguet, C. *Curr. Opin. Colloid Interface Sci.* **2006**, *11*, 280–289.

(5) $\Delta G_{\mathrm{m,n}}^{\mathrm{M,L}} = -RT \ln \beta_{\mathrm{m,n}}^{\mathrm{M,L}}$ corresponds to the van't Hoff isotherm with standard state 1 M. See:Munro, D. *Chem. Br.* **1977**, *13*, 100–105 and references therein for a thorough discussion.

Published on Web 01/05/2010

selection of the most stable coordination complex under thermodynamic control, obviously requires (i) a maximum number of these favorable microscopic metal-binding site contributions (this simple deduction is known as the principle of maximum site occupancy)[1a,6] and (ii) the chemical optimization of each metal-binding site interaction (this second deduction is often referred to as the principle of stereochemical matching).[7] In this context, the three additional thermodynamic microscopic descriptors c^{eff}, $\Delta E^{\mathrm{M,M}}$, and $\Delta E^{\mathrm{L,L}}$ offer attractive opportunities for putting into perspective these two well-respected "ukazes" in coordination and metallo-supramolecular chemistry, which often discourage the rational design of a wealth of unexpected nanoscopic polynuclear structures, thus leaving an empty space for serendipity.[8] We note, however, that the opposite contributions of similar magnitudes brought by Coulombic and solvation effects within the homo-component interactions $\Delta E^{\mathrm{M,M}}$ and $\Delta E^{\mathrm{L,L}}$ usually produce negligible cooperative effects (slightly positive or negative). Consequently, these parameters do not significantly influence the formation of the target saturated complexes in solution ($|\Delta E^{\mathrm{M,M}}| \approx |\Delta E^{\mathrm{L,L}}| \ll |\Delta G^{\mathrm{M,L}}_{\mathrm{inter}}| = |-RT \ln(f_i^{\mathrm{M,L}})|$).[4,9] In contrast, the experimental values found for the effective molarity EM (i.e., the experimental term for the concept of effective concentration, c^{eff}, written in eq 2)[10] operating (i) in metal-mediated porphyrin arrays,[11] (ii) in multisite ligand-proteins aggregates,[3k,12] or (iii) in sophisticated electrostatic adducts[13] cover a large domain (10^{-4} < EM < 10^{2} M). Assuming a pure entropic origin for the effective concentration, the theory predicts $c^{\mathrm{eff}} \propto d^{-n}$ with $n = {}^{3}/_{2}$ for free joint chains and $n = 3$ for an optimized spacer, whereby d is the separation between the two connected binding sites responsible for the intramolecular macrocyclization.[3,12,14] Therefore, only closely spaced donor atoms joined by a short linker may give EM ≫ 1 M, a particular situation often referred to as the chelate effect, in which the intramolecular connection is energetically preferred over its intermolecular counterpart ($\Delta G^{\mathrm{M,L}}_{\mathrm{intra}} - \Delta G^{\mathrm{M,L}}_{\mathrm{inter}} = -RT \ln(\mathrm{EM}) < 0$).[15]

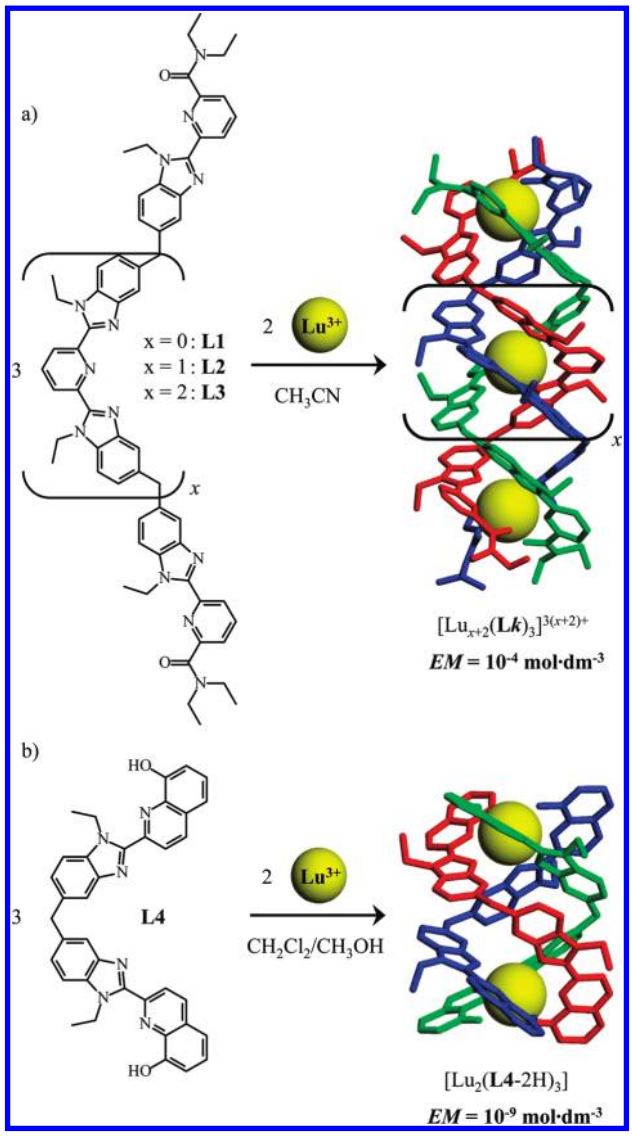

Figure 1. Self-asembly of lutetium triple-stranded polynuclear helicates with average effective molarities (EM) measured in solution for the macrocyclization of two adjacent binding sites.

It is thus not so suprising that triple-stranded polynuclear helicates $[\mathrm{Lu}_m(\mathbf{Lk})_3]^{3m+}$ (k = 1−3), in which two tridentate adjacent binding sites are separated by 9 Å and connected by semiflexible twisted diphenylmethane spacers, display (i) very limited preorganization for intramolecular macrocyclization and (ii) small effective molarities (EM = 10^{-4} M for the macrocyclization between two adjacent sites, Figure 1a).[9a] Interestingly, this parameter is extremely sensitive to minor enthalpic structural constraints, as illustrated by the removal of two degrees of rotational freedom in the terminal tridentate binding units in the ligand **L4**, which indeed reduces EM by 5 orders of magnitude (Figure 1b), while an obvious increase of EM is expected if we solely consider the entropic contribution.[16] Although not unambigously assigned to the sole variation of EM, the recent report of a decrease in magnitude on an order of 3 for the stability constants of

(6) (a) Lehn, J.-M.; Eliseev, A. V. *Science* **2001**, *291*, 2331–2333. (b) Hamacek, J.; Borkovec, M.; Piguet, C. *Chem. Eur. J.* **2005**, *11*, 5227–5237.
(7) (a) Piguet, C.; Bernardinelli, G.; Bocquet, B.; Quattropanni, A.; Williams, A. F. *J. Am. Chem. Soc.* **1992**, *114*, 7440–7451. (b) Lehn, J.-M. *Supramolecular Chemistry*; VCH: Weinheim, New York, Basel, Cambridge, Tokyo, 1995; p 142.
(8) Ward, M. D. *Chem. Commun.* **2009**, 4487–4499.
(9) (a) Riis-Johannessen, T.; Dalla Favera, N.; Todorova, T.; Huber, S. M.; Gagliardi, L.; Piguet, C. *Chem. Eur. J.* **2009**, 12702–12718. (b) Dalla Favera, N.; Guénée, L.; Bernardinelli, G.; Piguet, C. *Dalton Trans.* **2009**, 7625–7638.
(10) Mulder, A.; Huskens, J.; Reinhoudt, D. N. *Org. Biomol. Chem.* **2004**, *2*, 3409–3424. As recommended by Mulder et al., the term of effective molarity EM will be used for the experimental values, while the effective concentration, c^{eff}, will be used for the concept expressed in the mathematical equations. Please keep in mind that EM ≡ c^{eff} for numerical values.
(11) (a) Anderson, H. L.; Anderson, L.; Sanders, J. K. M. *J. Chem. Soc., Perkin Trans. 1* **1995**, 2231–2245. (b) Hunter, C. A.; Tomas, S. *J. Am. Chem. Soc.* **2006**, *128*, 8975–8979. (c) Ercolani, G. *Struct. Bonding* (*Berlin*) **2006**, *121*, 167–215. (d) Chekmeneva, E.; Hunter, C. A.; Packer, M. J.; Turega, S. M. *J. Am. Chem. Soc.* **2008**, *130*, 17718–17725. (e) Gonzalez-Alvarez, A.; Frontera, A.; Ballester, P. *J. Phys. Chem. B* **2009**, *113*, 11479–11489.
(12) Krishnamurthy, V. M.; Semetey, V.; Bracher, P. J.; Shen, N.; Whitesides, G. M. *J. Am. Chem. Soc.* **2007**, *129*, 1312–1320.
(13) Badjic, J. D.; Nelson, A.; Cantrill, S. J.; Turnbull, W. B.; Stoddart, J. F. *Acc. Chem. Res.* **2005**, *38*, 723–732.
(14) Dalla Favera, N.; Hamacek, J.; Borkovec, M.; Jeannerat, D.; Gumy, F.; Bünzli, J.-C. G.; Ercolani, G.; Piguet, C. *Chem. Eur. J.* **2008**, *14*, 2994–3005.
(15) (a) Simmons, E. L. *J. Chem. Educ.* **1979**, *56*, 578–579. (b) Motekaitis, R. J.; Martell, A. E.; Hancock, R. A. *Coord. Chem. Rev.* **1994**, *133*, 39–65. (c) Hunter, C. A.; Anderson, H. L. *Angew. Chem., Int. Ed.* **2009**, *48*, 7488–7499.
(16) Terazzi, E.; Guénée, L.; Bocquet, B.; Lemonnier, J.-F.; Dalla Favera, N.; Piguet, C. *Chem. Eur. J.* **2009**, *15*, 12719–12732.

Scheme 1. Chemical Structures of Ligands **L5**−**L8**

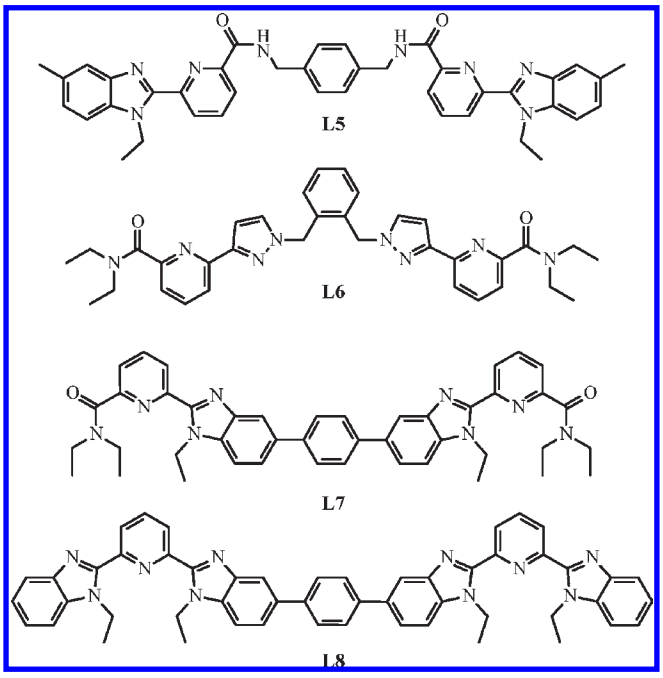

mononuclear lanthanide complexes, in which the ethylene spacer has been replaced with peptides of variable lengths, suggests that the effective molarity is also amenable to significant modulation when the spacer is systematically varied.[17] Since $\Delta G^{M,L}_{intra} - \Delta G^{M,L}_{inter} = -RT \ln (EM) = 51$ kJ mol^{-1} for EM = 10^{-9} M (standard state 1 M),[5,15b] this parameter indeed represents a considerable contribution to the global free energy change accompanying the assembly process. In this context, the unexpected isolation of the trinuclear circular single-stranded helicates $[Ln_3(\mathbf{L5})_3(CF_3SO_3)_4]^{5+}$ [18] or the formation of bridged binuclear side-by side complexes $[Ln_2(\mathbf{L6})_2(\mu\text{-}CH_3CO_2)(H_2O)_2]^{5+}$ [19] instead of the planned saturated bicyclic binuclear triple-stranded helicates $[Ln_2(\mathbf{L}k)_3]^{6+}$ upon reaction of the constrained ligands **L5** and **L6** with trivalent lanthanides, Ln(III), in a Ln:**L** = 2:3 ratio could be the result of systems minimizing some unfavorable intramolecular connections (Scheme 1 and Figure S1, Supporting Information). However, the last two observations entirely rely on solid-state structures obtained by serendipity with no direct access to the thermodynamic parameters controlling the chemical assembly occurring in solution. The question thus arises about a possible rational programming of polynuclear complexes, for which the speciation obtained under thermodynamic control deliberately deviates from the two classical principles of (i) maximum site occupancy and (ii) stereochemical matching, without resorting to the formation of ternary complexes with highly competitive solvent molecules or counteranions.[8,20]

In this contribution, we build on this reasoning with the design of the bis-tridentate ligands **L7** and **L8** (Scheme 1), in which (i) the rotational degrees of freedoms are restricted to

Scheme 2. Synthetic Strategy for the Preparation of Ligands **L7** and **L8** with Numbering Scheme for ^{1}H NMR

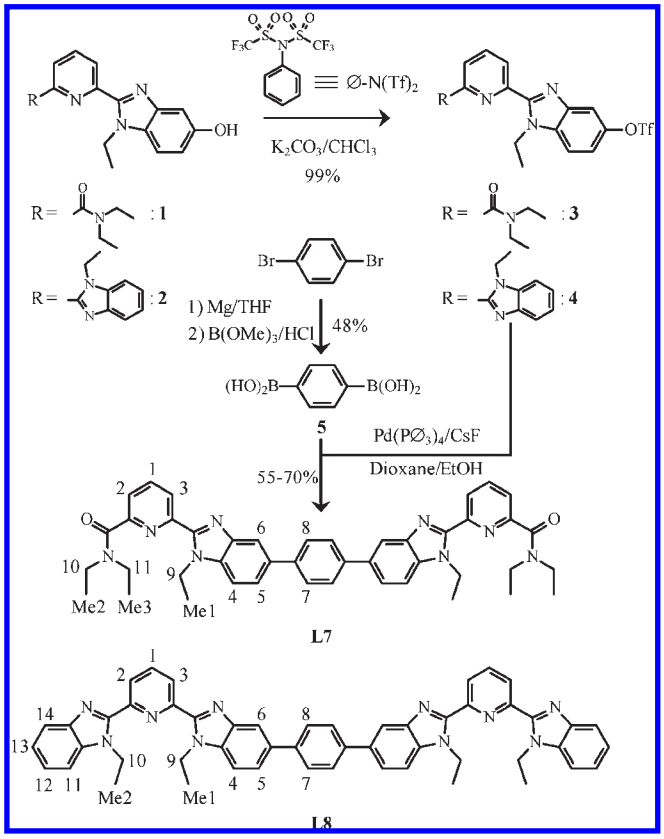

interannular rotations about $C_{aromatic}-C_{aromatic}$ bonds and (ii) the flexibility of the spacer is limited by the central rigid phenyl ring. We thus expect effective molarities upon complexation to trivalent lanthanides so small that the saturated triple-stranded helicates $[Ln_2(\mathbf{L}k)_3]^{6+}$ (k = 7, 8), obeying both principles of maximum site occupancy and of stereochemical matching, cannot be formed in solution under accessible concentrations at Ln:**L***k* = 2:3 stoichiometric ratio.

Results and Discussion

Syntheses and Structures of the Constrained Ligands L7 and L8. In comparison with **L5** and **L6**, the removal of some rotational degrees of freedom in the phenyl spacer used in **L7** and **L8** requires the formation of $C_{arom}-C_{arom}$ bonds via a Miyaura−Suzuki strategy.[21] Among the various criteria of reactivity favoring this coupling reaction, the optimum situation requires the use of a polar solvent,[22] an electron-poor aromatic ring bearing the C−X bond (X = halogen, pseudohalogen), an electron-rich aromatic boronic acid,[23] and the addition of a poorly hydrolyzing base, such as carbonate or fluoride.[24]

For synthetic reasons,[25] the Suzuki coupling reactions connecting two peripheral benzimidazole rings to the

(17) Cisnetti, F.; Gateau, C.; Lebrun, C.; Delangle, P. *Chem. Eur. J.* **2009**, *15*, 7456–7469.
(18) Senegas, J.-M.; Koeller, S.; Piguet, C. *Chem. Commun.* **2005**, 2235–2237.
(19) Ronson, T. K.; Adams, H.; Harding, L. P.; Pope, S. J. A.; Sykes, D.; Faulkner, S.; Ward, M. D. *Dalton Trans.* **2007**, 1006–1022.
(20) Escande, A.; Guénée, L.; Buchwalder, K.-L.; Piguet, C. *Inorg. Chem.* **2009**, *48*, 1132–1147.
(21) (a) Miyaura, N.; Suzuki, A. *Chem. Rev.* **1995**, *95*, 2457–2483. (b) Stanforth, S. P. *Tetrahedron* **1998**, *54*, 263–303. (c) Tobisu, M.; Chatani, N. *Angew. Chem., Int. Ed.* **2009**, *48*, 3565–3568.
(22) Roger, J.; Doucet, H. *Org. Biomol. Chem.* **2008**, *6*, 169–174.
(23) Liu, S.-Y.; Choi, M. J.; Fu, G. C. *Chem. Commun.* **2001**, 2408–2409.
(24) Campeau, L.-C.; Fagnou, K. *Chem. Soc. Rev.* **2007**, *36*, 1058–1068.
(25) Nozary, H.; Piguet, C.; Tissot, P.; Bernardinelli, G.; Bünzli, J.-C. G.; Deschenaux, R.; Guillon, D. *J. Am. Chem. Soc.* **1998**, *120*, 12274–12288.

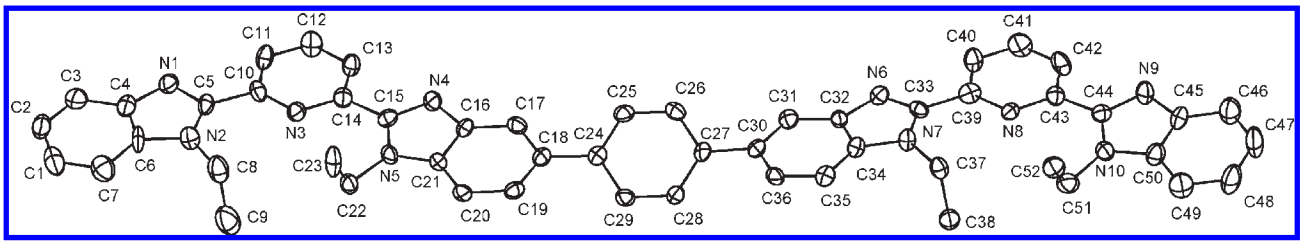

Figure 2. Perspective view with numbering scheme of the molecular structure of **L8** in the crystal structure of **L8**·3$CHCl_3$. Ellipsoids are represented at the 50% probability level.

para positions of the central phenyl ring in **L7** and **L8** (Scheme 2) deal with the unfavorable combination of electron-rich triflate acceptors (**3** and **4**) with the electron-deficient bis-boronic acid **5**. We were thus forced to develop a smooth methodology for the selective transfer of a triflate group onto the hydroxybenzimidazole rings **1** and **2** without producing either ring opening[26] or N- versus O-alkylation.[27] For this purpose, we first optimized the reaction of *N*-phenyl-bistriflimide (Ø-N-$(Tf)_2$, Scheme 2)[28] with the easily accessible hydroxybenzimidazole scaffold **S6** (Scheme S1, Figure S2, and Table S1 in the Supporting Information). Once **3** or **4** could be obtained from **1** and **2** with this technique (Scheme 2), their Suzuki coupling with **5** then simply used a Pd(0) catalyst in dioxane/ethanol with CsF as a source of fluoride. The ^{1}H NMR spectra of **L7** and **L8** (Figure 3a and Figure S9a and Tables S3 and S4 in the Supporting Information) indicate 2-fold symmetries in solution (i.e., two equivalent tridentate binding units) combined with mirror planes responsible for the systematic observation of enantiotopic methylene protons (H9,9′, H10,10′, and H11,11′ in **L7**; H9,9′ and H10,10′ in **L8**). None of the four blocked conformations of the bis-benzimidazole-phenyl spacer, compatible with C_{2h} or C_{2v} symmetry in solution (Scheme S2, Supporting Information), indeed correspond to the crystal structure of **L8**·3$CHCl_3$ (Figure 2), which displays an intermediate situation with interplanar benzimidazole−phenyl angles of 26.0(2) and 34.2(2)° (Table S2, Supporting Information). This arrangement corresponds to the best compromise for minimizing steric hindrance produced by the four hydrogen atoms occupying the ortho positions around the $C_{bzim}-C_{phenyl}$ bond, while retaining some favorable π overlap between the three conjugated aromatic rings of the spacer. Moreover, the pyridine and benzimidazole rings of **L8** take part in intermolecular aromatic stacking interactions in the crystal lattice, which further produce distortions in the solid state (Figure S3, Supporting Information). We conclude that the apparent C_{2h} or C_{2v} symmetries observed in solution result from fast rotations about the $C_{bzim}-C_{phenyl}$ bonds in **L7** and **L8** on the NMR time scale. We also note that the approximately planar tridentate bis-benzimidazole pyridine binding units in **L8** (interplanar benzimidazole−pyridine angles: 5.2−11.2°, Table S2) adopt the expected trans,trans arrangement of the three coordinating N-donors, which minimizes dipole moments (Figure 2).

Complexation and Speciation of L7 and L8 with Trivalent Lanthanide Triflates in Solution. Electrospray ionization-mass spectrometric (ESI-MS) titrations of **L7** (10^{-4} M in CH_2Cl_2/CH_3CN (9:1)) with $Eu(CF_3SO_3)_3\cdot 3H_2O$ (Eu:**L7** = 0.1:3.0) exclusively shows the existence in the gas phase of the complexes $[Eu_2(\mathbf{L7})_2(CF_3SO_3)_x(CH_3CN)_y]^{(6-x)+}$ (x = 2−4, y = 1−3) possessing a 2:2 stoichiometry, with the base peak of the spectra corresponding to $[Eu_2(\mathbf{L7})_2(CF_3SO_3)_4]^{2+}$. Parallel ^{1}H NMR titrations of **L7** (10^{-2} M in $CDCl_3/CD_3CN$ (1:1)) with $Ln(CF_3SO_3)_3\cdot xH_2O$ (Ln = La, Eu, Lu, Y; x = 4, 5) show the fadeout of the signals of the free ligand, which are replaced with patterns diagnostic for the successive formations of $[Ln_2(\mathbf{L7})_2]^{6+}$ (2:2 stoichiometry) and $[Ln_2(\mathbf{L7})]^{6+}$ (2:1 stoichiometry, Figure 3 and Figures S4−S7 in the Supporting Information). Interestingly, no trace (limit of detection < 5%) of the saturated triple-stranded helicate $[Ln_2(\mathbf{L7})_3]^{6+}$ (2:3 stoichiometry) could be observed by ^{1}H NMR. Except for some specific broadening associated with La(III) (intermediate exchange rate on the NMR time scale, Figure S4),[9b] or Eu(III) (paramagnetic induced nuclear relaxation, Figure S5),[29] the ^{1}H NMR spectra recorded for Ln:**L7** = 1.0 and 2.0 (Ln = La, Eu, Lu, Y) are diagnostic for the formation of twisted D_2-symmetrical double-stranded helicates $[Ln_2(\mathbf{L7})_2]^{6+}$ (Figure 3b) and planar C_{2v}-symmetrical complexes $[Ln_2(\mathbf{L7})]^{6+}$ (Figure 3c). Two-dimensional $\{^1H-^1H\}$-COSY NMR spectra allow the complete assignment of all signals (Table S3, Supporting Information), thus confirming that the 2-fold symmetry of the ligand is retained in both complexes (Figure 3). In $[Ln_2(\mathbf{L7})_2]^{6+}$, the diastereotopic character of the methylene protons (H9, H10, and H11; doublet of quartets with $^2J = 2(^3J) = 14$ Hz, Figure 3b) precludes the existence of symmetry planes passing through the ligand backbone, in agreement with a D_2-symmetrical double-stranded organization of the strands but incompatible with the formation of a planar macrocyclic binuclear complex. In $[Ln_2(\mathbf{L7})]^{6+}$, the restoration of well-resolved quartets for the enantiotopic methylene protons H9, H10, and H11 (Figure 3c) implies an average planar arrangement of the ligand strand on the NMR time scale.

A close scrutiny at the ^{1}H NMR titration data (Figures S4−S7, Supporting Information) shows the chemical shift of residual water to abruptly vary for Ln:**L7** > 1, which indicates that fast exchange of water molecules in

(26) Couladouros, E. A.; Moutsos, V. I.; Lampropoulou, M.; Little, J. L.; Hyatt, J. A. *J. Org. Chem.* **2007**, *72*, 6735–6741.
(27) Cottyn, B.; Vichard, D.; Terrier, F.; Nioche, P.; Raman, C. S. *Synlett* **2007**, *8*, 1203–1206.
(28) Hendrikson, J. B.; Bergeron, R. *Tetrahedron Lett.* **1973**, *43*, 4607–4610.
(29) Piguet, C.; Geraldes, C. F. G. C. In *Handbook on the Physics and Chemistry of Rare Earths*; Gschneidner, K. A., Jr, Bünzli, J.-C. G., Pecharsky, V. K., Eds.; Elsevier Science: Amsterdam, 2003; Vol. *33*, pp 353−463.

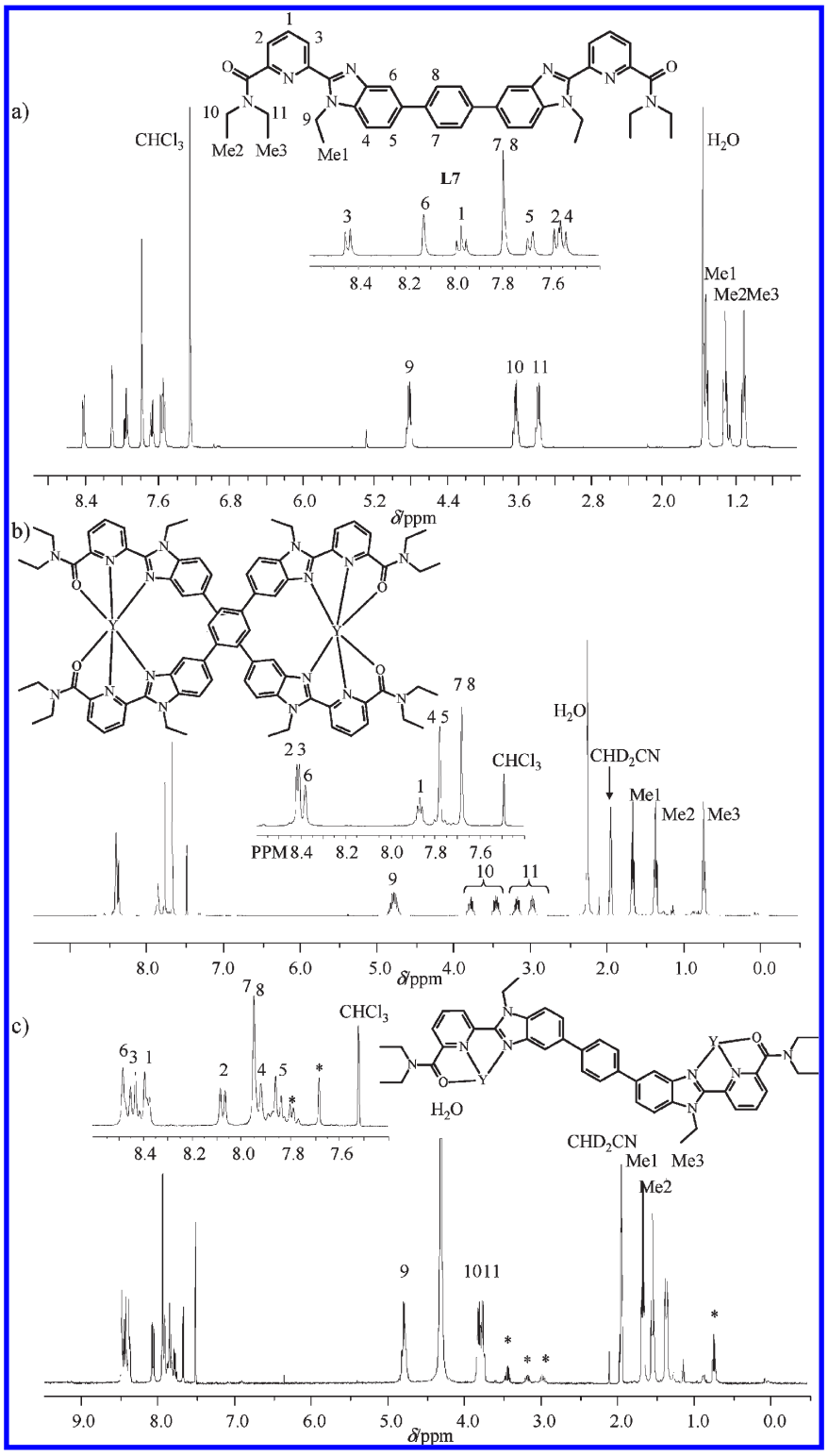

Figure 3. 400 MHz ^{1}H NMR spectra of (a) **L7**, (b) $[Y_2(\mathbf{L7})_2]^{6+}$, and (c) $[Y_2(\mathbf{L7})]^{6+}$ (asterisks denote traces of $[Y_2(\mathbf{L7})_2]^{6+}$) in $CDCl_3/CD_3CN$ (1:1) at 298 K.

the first coordination sphere only occur for the single-stranded complexes $[Ln_2(\mathbf{L7})]^{6+}$. Complementary ^{19}F NMR data show a single signal for the counteranion $CF_3SO_3^-$ along the complete titrations, in line with either purely ionic behavior, or fast exchange in the first coordination sphere for both complexes. Very similar results are obtained for **L8** (Figures S8 and S9 and Table S4, Supporting Information), which establish the successive formation of the D_2-symmetrical double-stranded helicates $[Ln_2(\mathbf{L8})_2]^{6+}$ followed by the planar C_{2v}-symmetrical complexes $[Ln_2(\mathbf{L8})]^{6+}$. As expected, the treatment of $[Ln_2(\mathbf{L8})_2]^{6+}$ with optically pure Δ-Trisphat anion (6 equiv)[30] splits some aromatic ^{1}H NMR signals (Figure S10, Supporting Information), which ultimately demonstrates the formation of equal quantities of the two

(30) Lacour, J.; Ginglinger, C.; Favarger, F.; Torche-Haldimann, S. *Chem. Commun.* **1997**, 2285–2286.

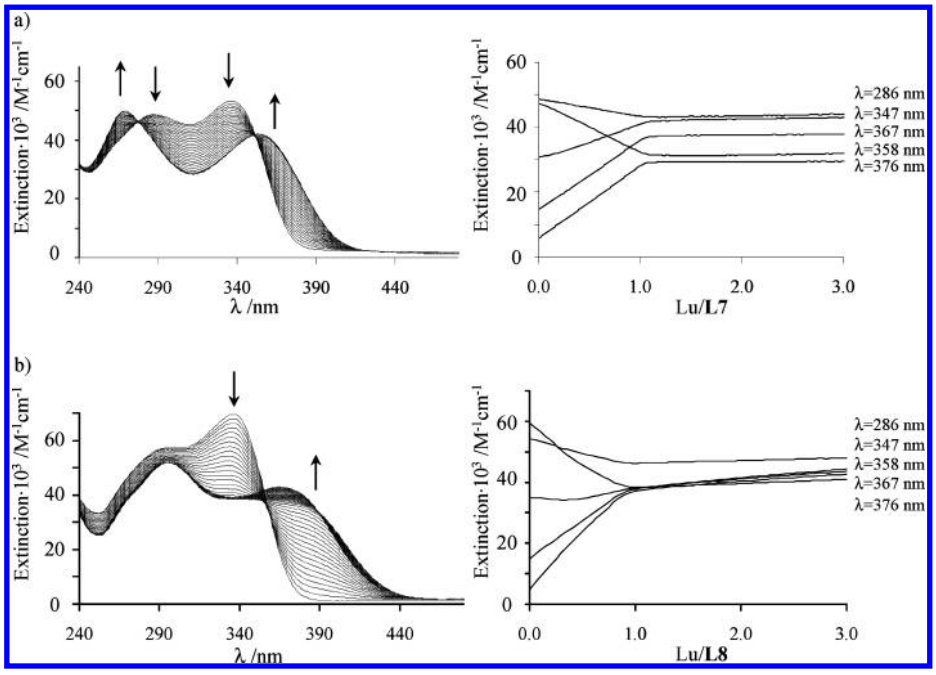

Figure 4. Variation of molar extinction observed during the spectrophotometric titrations of (a) **L7** with $Lu(CF_3SO_3)_3 \cdot 4H_2O$ and (b) **L8** with $Lu(CF_3SO_3)_3 \cdot 4H_2O$ (298 K, CH_2Cl_2/CH_3CN 1:1, total ligand concentration 10^{-4} M).

enantiomers of the D_2-symmetrical double-stranded helicate Δ,Δ-$[Ln_2(\mathbf{L8})_2]^{6+}$ and Λ,Λ-$[Ln_2(\mathbf{L8})_2]^{6+}$ in slow exchange on the NMR time scale. The formation of the alternative achiral C_{2h}-symmetrical side-by-side complex Λ,Δ-$[Ln_2(\mathbf{L8})_2]^{6+}$ (sometimes called mesocate)[31b] can be thus excluded once and for all. The only remarkable difference between the complexation of **L7** and **L8** concerns the quantitative transformation of $[Ln_2(\mathbf{L8})_2]^{6+}$ into $[Ln_2(\mathbf{L8})]^{6+}$ for Ln:**L8** = 2:1 for a total ligand concentration of 10 mM (Figure S9c, Supporting Information), while both complexes coexist in solution for **L7** under the same conditions (Figure 3c).

The latter observation suggests different thermodynamic behaviors, which are unraveled by using spectrophotometric titrations of **L7** or **L8** (10^{-4} M in CH_2Cl_2/CH_3CN 1:1) with $Ln(CF_3SO_3)_3 \cdot xH_2O$ (Ln = La, Eu, Lu, Y; x = 2−4; Ln:**L*k*** = 0.1−3.0; Figure 4). The variation of the absorption spectra, which mainly results from the electronic reorganization of the π system upon trans,trans to cis,cis conformational change of the tridentate binding units due to complexation to Ln(III),[32] systematically shows one pronounced end point for Ln:**L*k*** = 1.0, followed by a smooth evolution for Ln:**L*k*** > 1.0 (Figure 4). Factor analysis[33] indicates the interconversion of three absorbing species assigned to **L*k***, $[Ln_2(\mathbf{Lk})_2]^{6+}$, and $[Ln_2(\mathbf{Lk})]^{6+}$ in agreement with ESI-MS and NMR titrations. The global set of spectrophotometric data can be satisfyingly fitted with equilibria (3) and (4) by using nonlinear least-squares techniques.[34] The associated cumulative stability constants $\beta_{2,n}^{Ln,Lk}$ are collected in Table 1.[35]

$$2\mathbf{Lk} + 2[Ln(CH_3CN)_9]^{3+} \rightleftharpoons [Ln_2(\mathbf{Lk})_2(CH_3CN)_6]^{6+} + 12CH_3CN \quad \beta_{2,2}^{Ln,\mathbf{Lk}} \tag{3}$$

$$\mathbf{Lk} + 2[Ln(CH_3CN)_9]^{3+} \rightleftharpoons [Ln_2(\mathbf{Lk})(CH_3CN)_{12}]^{6+} + 6CH_3CN \quad \beta_{2,1}^{Ln,\mathbf{Lk}} \tag{4}$$

For the all-nitrogen ligand **L8**, the calculated electronic absorption spectra of the complexes $[Ln_2(\mathbf{L8})_2]^{6+}$ and $[Ln_2(\mathbf{L8})]^{6+}$ are sufficiently different for allowing acceptable noncorrelated values for $\beta_{2,2}^{Ln,\mathbf{L8}}$ and $\beta_{2,1}^{Ln,\mathbf{L8}}$, an assertion substantiated by the good match between direct integration of the experimental ^{1}H NMR data recorded during titration at 10^{-2} M and the computed speciation predicted by using the stability constants of Table 1 (entries 5 and 6 in Table 1 and Figure S11, Supporting Information). However, the situation is less favorable for **L7**, because the replacement of terminal benzimidazole groups with carboxamide units provides almost identical absorption spectra for $[Ln_2(\mathbf{L7})_2]^{6+}$ and $[Ln_2(\mathbf{L7})]^{6+}$. Consequently, the fitted values obtained by spectrophotometry for $\beta_{2,2}^{Ln,\mathbf{L7}}$ and $\beta_{2,1}^{Ln,\mathbf{L7}}$ are strongly correlated and

(31) (a) Piguet, C.; Bernardinelli, G.; Hopfgartner, G. *Chem. Rev.* **1997**, *97*, 2005–2062. (b) Albrecht, M. *Chem. Rev.* **2001**, *101*, 3457–3497.

(32) Piguet, C.; Bünzli, J.-C. G.; Bernardinelli, G.; Bochet, C. G.; Froidevaux, P. *J. Chem. Soc., Dalton Trans.* **1995**, 83–97.

(33) Malinowski, E. R.; Howery, D. G. *Factor Analysis in Chemistry*; Wiley,: New York, Chichester, 1980.

(34) (a) Gampp, H.; Maeder, M.; Meyer, C. J.; Zuberbühler, A. *Talanta* **1985**, *32*, 1133–1139. (b) Gampp, H.; Maeder, M.; Meyer, C. J.; Zuberbühler, A. *Talanta* **1986**, *33*, 943–951.

(35) For the sake of simplicity when calculating symmetry numbers (Figure S13, Supporting Information), we consider that Ln(III) exists in acetonitrile strictly as the tricapped-trigonal-prismatic solvates $[Ln(CH_3CN)_9]^{3+}$, although it has been experimentally demonstrated that the main species in equilibrium for lanthanide triflate solutions in anhydrous acetonitrile are $[Ln(Otf)_2(CH_3CN)_x]^+$ and $[Ln(Otf)_3(CH_3CN)_y]$; see: Di Bernardo, P.; Choppin, G. R.; Portanova, R.; Zanonato, P. L. *Inorg. Chim. Acta* **1993**, *207*, 85–91. Alternative geometries have been considered, but the changes in symmetry numbers have very little effect on the final microscopic descriptors.

Table 1. Experimental Cumulative Formation Constants log ($\beta_{2,n}^{Ln,Lk}$) (k = 7, 8) and log ($\beta_{1,n}^{Ln,Lk}$) (k = 9, 10) Obtained by Spectrophotometry According to Equilibria (3)−(4) and (7)−(9) for the Complexes $[Ln_2(\mathbf{Lk})_n]^{6+}$ (k = 7, 8) and $[Ln(\mathbf{Lk})_n]^{3+}$ (k = 9, 10; Ln = La, Eu, Lu, Y; 1:1 CH_2Cl_2/CH_3CN, 298 K)

	Ln(III)			
	La	Eu	Y	Lu
$R_{Ln}^{CN=9}$/Å[a]	1.216	1.120	1.075	1.032
$\log \beta_{2,2}^{Ln,L7}$	18.7(4)	19.4(6)	19.7(6)	19.6(9)
$\log \beta_{2,1}^{Ln,L7}$	13.0(4)	12.3(5)	13.1(4)	12.0(7)
$\log \beta_{2,1}^{Ln,L7}$[b]	11.5(3)	11.0(3)	11.2(3)	11.0(3)
$\log \beta_{2,2}^{Ln,L8}$	17.8(2)	16.7(1)	17.2(3)	17.4(3)
$\log \beta_{2,1}^{Ln,L8}$	12.0(1)	10.9(1)	11.8(2)	11.2(3)
$\log \beta_{1,1}^{Ln,L9}$	7.4(3)	8.2(4)	7.9(6)	7.5(5)
$\log \beta_{1,2}^{Ln,L9}$	14.5(4)	14.9(6)	15.3(8)	14.9(7)
$\log \beta_{1,3}^{Ln,L9}$	20.9(5)	21.6(7)	23(1)	21.8(9)
$\log \beta_{1,1}^{Ln,L10}$	7.9(4)	7.8(4)	7.7(3)	8.1(3)
$\log \beta_{1,2}^{Ln,L10}$	14.6(5)	14.2(6)	14.3(5)	14.7(4)
$\log \beta_{1,3}^{Ln,L10}$	21.5(7)	20.7(8)	21.2(7)	19.9(7)

[a] Ionic radii for nine-coordinate trivalent lanthanides.[43] [b] Estimated from ^{1}H NMR titrations (see text).

pseudoisosbestic points are indeed observed during the titration processes (Figure 4a). A detailed analysis of the nonlinear least-squares fit process shows that convergence is very sensitive to the values of $\beta_{2,2}^{Ln,L7}$, which can be thus satisfyingly obtained from spectrophotometric data, but $\beta_{2,1}^{Ln,L7}$ can be varied within a rather wide range without significantly influencing the fitting process. The comparison between direct integration of the experimental ^{1}H NMR data recorded during titration at 10^{-2} M (Figure S12a, Supporting Information) and the computed speciation obtained by using the stability constants of Table 1 (entries 2 and 3 in Table 1 and Figure S12b, Supporting Information) indeed shows considerable discrepancies. Fixing $\beta_{2,2}^{Ln,L7}$ at their values obtained by spectrophotometry allows the fit of a second set of more reliable $\beta_{2,1}^{Ln,L7}$ values by using the NMR data (entry 4 in Table 1), which eventually provides a very good match between experimental and computed speciations in the whole experimentally accessible concentration range (10^{-4}−10^{-1} M; Figure S12c, Supporting Information). We are now in a position to reliably compare the stability constants found for the two different bis-tridentate ligands. First, $\beta_{2,1}^{Ln,L7} \simeq \beta_{2,1}^{Ln,L8}$ obtained for the single-stranded binuclear complexes $[Ln_2(\mathbf{Lk})]^{6+}$ indicates that the intermolecular affinities of the tridentate N_2O or N_3 binding sites for Ln(III) are similar, as previously established by a thorough analysis of the triple-stranded helicates produced with ligands **L1**−**L3**.[9a,14] Second, $\beta_{2,2}^{Ln,L7} > \beta_{2,2}^{Ln,L8}$ (2 orders of magnitude) implies that the macrocyclization required for the formation of the double-stranded helicate is less favorable for the more bulky ligand **L8**, again in line with previous observations reported for related triple-stranded binuclear triple-stranded helicates fitted with the N_2O or N_3 binding units used in this work.[36] The different behavior between **L7** and **L8** is responsible for the concomitant observation of $[Ln_2(\mathbf{L7})_2]^{6+}$ and $[Ln_2(\mathbf{L7})]^{6+}$ complexes in solution by NMR for Ln:**L7** = 2:1 (total ligand concentration 10^{-2} M; Figure 3c), while only $[Ln_2(\mathbf{L8})]^{6+}$ is detected under the same conditions (Figure S9c, Supporting Information). Finally, the most striking point concerns the nondetection of the saturated triple-stranded helicates $[Ln_2(\mathbf{Lk})_3]^{6+}$ (k = 7, 8) within the 10^{-1}−10^{-4} M concentration range, although the latter complexes correspond to the only candidates satisfying simultaneously (i) the principle of maximum site occupancy and (ii) the principle of stereochemical matching.

(36) (a) Piguet, C.; Bünzli, J.-C. G.; Bernardinelli, G.; Hopfgartner, G.; Williams, A. F. *J. Am. Chem. Soc.* **1993**, *115*, 8197–8206. (b) Zeckert, K.; Hamacek, J.; Rivera, J.-P.; Floquet, S.; Pinto, A.; Borkovec, M.; Piguet, C. *J. Am. Chem. Soc.* **2004**, *126*, 11589–11601.

Scheme 3. Chemical Structures of Ligands **L9** and **L10**

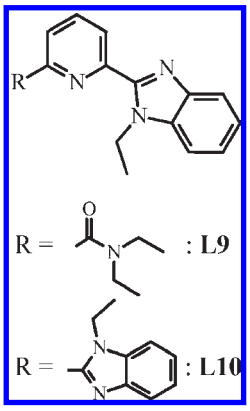

Thermodynamics, Effective Molarities, and Quantitative Deviations from the Standard Principles. Application of the site binding model (eq 2) to equilibria (3) and (4) gives eqs 5 and 6, in which a set of four different microscopic descriptors is involved ($f_{\mathbf{Lk}}^{Ln}$, $u^{\mathbf{Lk},\mathbf{Lk}}$, $u_{\mathbf{Lk}}^{Ln,Ln}$ and $c_{double}^{eff,\mathbf{Lk}}$ with k = 7, 8; the statistical factors are calculated and reported in Figure S13 (Supporting Information).[35]

$$\beta_{2,2}^{Ln,\mathbf{Lk}} = 72(f_{\mathbf{Lk}}^{Ln})^4(u^{\mathbf{Lk},\mathbf{Lk}})^2(u_{\mathbf{Lk}}^{Ln,Ln})(c_{double}^{eff,\mathbf{Lk}}) \quad (5)$$

$$\beta_{2,1}^{Ln,\mathbf{Lk}} = 36(f_{\mathbf{Lk}}^{Ln})^2(u_{\mathbf{Lk}}^{Ln,Ln}) \quad (6)$$

An elegant strategy for estimating experimental values for these parameters requires additional information obtained by the spectrophotometric determination of additional stability constants with ligands **L9** and **L10**, which respectively possess tridentate N_2O and N_3 binding units identical with those found in **L7** and **L8** (Scheme 3, equilibria 7−9, k = 9, 10, Table 1).

$$\mathbf{Lk} + [Ln(CH_3CN)_9]^{3+} \rightleftharpoons [Ln(\mathbf{Lk})(CH_3CN)_6]^{3+} + 3CH_3CN \quad \beta_{1,1}^{Ln,\mathbf{Lk}} \quad (7)$$

$$2\mathbf{Lk} + [Ln(CH_3CN)_9]^{3+} \rightleftharpoons [Ln(\mathbf{Lk})_2(CH_3CN)_3]^{3+} + 6CH_3CN \quad \beta_{1,2}^{Ln,\mathbf{Lk}} \quad (8)$$

$$3\mathbf{Lk} + [Ln(CH_3CN)_9]^{3+} \rightleftharpoons [Ln(\mathbf{Lk})_3]^{3+} + 9CH_3CN \quad \beta_{1,3}^{Ln,\mathbf{Lk}} \quad (9)$$

Reasonably assuming that (i) a single average value for the intermetallic interaction ($u_{\mathbf{Lk}}^{Ln,Ln}$) is considered for

$[Ln_2(\mathbf{L}k)_2]^{6+}$ and $[Ln_2(\mathbf{L}k)]^{6+}$, (ii) the absolute intermolecular affinities of the tridentate binding sites for Ln(III) ($f^{Ln}_{\mathbf{L}k}$) are identical for the **L7**/**L9** ($f^{Ln}_{\mathbf{L7}} = f^{Ln}_{\mathbf{L9}} = f^{Ln}_{N2O}$) and **L8**/**L10** ($f^{Ln}_{\mathbf{L8}} = f^{Ln}_{\mathbf{L10}} = f^{Ln}_{N3}$) pairs, and (iii) so are the interligand interactions ($u^{\mathbf{L7},\mathbf{L7}} = u^{\mathbf{L9},\mathbf{L9}} = u^{N2O,N2O}$ and $u^{\mathbf{L8},\mathbf{L8}} = u^{\mathbf{L10},\mathbf{L10}} = u^{N3,N3}$, the application of the site binding model to equilibria 7−9 provides the six additional equations (10)−(15).[37]

$$\beta^{Ln,\mathbf{L9}}_{1,1} = 6f^{Ln}_{N2O} \quad (10)$$

$$\beta^{Ln,\mathbf{L9}}_{1,2} = 6(f^{Ln}_{N2O})^2(u^{N2O,N2O}_{HH} + u^{N2O,N2O}_{HT}) \quad (11)$$

$$\beta^{Ln,\mathbf{L9}}_{1,3} = (f^{Ln}_{N2O})^3(4(u^{N2O,N2O}_{HH})^3 + 12(u^{N2O,N2O}_{HT})^2(u^{N2O,N2O}_{HH})) \quad (12)$$

$$\beta^{Ln,\mathbf{L10}}_{1,1} = 6f^{Ln}_{N3} \quad (13)$$

$$\beta^{Ln,\mathbf{L10}}_{1,2} = 12(f^{Ln}_{N3})^2u^{N3,N3} \quad (14)$$

$$\beta^{Ln,\mathbf{L10}}_{1,3} = 16(f^{Ln}_{N3})^3(u^{N3,N3})^3 \quad (15)$$

The two parameters $u^{N2O,N2O}_{HH}$ and $u^{N2O,N2O}_{HT}$ in eqs 11 and 12 results from the lack of C_2 symmetry in **L9**,[16] which produces head-to-head (HH) or head-to-tail (HT) orientations when coordinated to the same metal ions. If we assume that there is no difference in energy between the two possible orientations, i.e. $u^{N2O,N2O}_{HH} = u^{N2O,N2O}_{HT} = u^{N2O,N2O}$, eqs 10−12 resume to eqs 13−15 except for the replacement of f^{Ln}_{N3} with f^{Ln}_{N2O}. Under these conditions, we expect purely entropic 1:1 ratios for HH-$[Ln(\mathbf{L9})_2]^{3+}$/HT-$[Ln(\mathbf{L9})_2]^{3+}$ and 1:3 ratios for HHH-$[Ln(\mathbf{L9})_3]^{3+}$/HHT-$[Ln(\mathbf{L9})_3]^{3+}$ isomers in solution, a distribution very close to the experimental speciations previously reported for these complexes in acetonitrile at 298 K.[38] Therefore, we finally performed simple multilinear least-squares fits of eqs 5, 6, and 13−15 (five equations) for each type of tridentate binding units (N_2O or N_3) in order to determine the two sets of four microscopic thermodynamic parameters collected in Table 2 and graphically shown in Figure 5.

First, the stability constant computed with eqs 5, 6, and 13−15 and using the microscopic parameters of Table 2 satisfyingly reproduce the experimental data ($0.001 \leq AF_{Ln} \leq 0.01$).[39] Second, the interligand ($\Delta E^{L,L}$) and intermetallic ($\Delta E^{Ln,Ln}$) interactions and the intermolecular connections $\Delta G^{Ln,L}_{inter} = -RT \ln f^{Ln}_{L}$ are very similar for both type of binding units (N_2O or N_3). Moreover, they do not significantly vary along the lanthanide series within experimental errors, as previously reported for the polynuclear triple-stranded helicates $[Ln_m(\mathbf{L}k)_3]^{3m+}$ ($k = 1-3$, $m = 2-4$).[9a,14] Though the interligand interactions are close to negligible ($-1 \leq \Delta E^{L,L} \leq 6$ kJ mol^{-1}), the average magnitude of the intermetallic interaction $\Delta E^{Ln,Ln} = 24(4)$ kJ mol^{-1} found in $[Ln_2(\mathbf{L7})_n]^{6+}$ and $[Ln_2(\mathbf{L8})_n]^{6+}$ is much larger than $\Delta E^{Ln,Ln} = 4(1)$ kJ mol^{-1} found for $[Ln_m(\mathbf{L}k)_3]^{3m+}$ ($k = 1-3$, $m = 2-4$) in acetonitrile, whereby the intermetallic distance amounts to 9 Å.[9a] Contrary to simple predictions solely based on the Coulomb equation, an increase in $\Delta E^{Ln,Ln}$ for solvated polynuclear helicates implies an increase in the intermetallic separation because of the reduction of the favorable free energies of solvation in larger molecular objects.[9b,40] We thus predict that the Ln···Ln intrahelical distances significantly exceed 9 Å in $[Ln_2(\mathbf{L7})_n]^{6+}$ and $[Ln_2(\mathbf{L8})_n]^{6+}$. However, the most striking difference between the latter double-stranded helicates ($n = 2$) and the analogous triple-stranded complexes $[Ln_m(\mathbf{L}k)_3]^{3m+}$ ($k = 1-3$, $m = 2-4$) relies on the minute values of the effective molarities ($10^{-6.3} \leq EM^{Ln,\mathbf{L7}}_{double} \leq 10^{-5.5}$ M and $10^{-8} \leq EM^{Ln,\mathbf{L8}}_{double} \leq 10^{-6.6}$ M; Table 2), in comparison with the average values $EM^{Lu,\mathbf{L1}} = 10^{-4}$ M previously estimated for the formation of multiple-stranded helicates $[Ln_m(\mathbf{L}k)_3]^{3m+}$ ($k = 1-3$, $m = 2-4$; Figure 1a).[9a] We thus deduce that the replacement of the methylene spacer in **L1** with a para-disubstituted phenyl ring in **L7** and **L8** reduces the preorganization for macrocyclization by 2−4 orders of magnitude, thus leading to intramolecular connection processes which are still slightly favorable for the N_2O binding units ($-10 \leq \Delta G^{Ln,\mathbf{L7}}_{intra} = -RT \ln$

Table 2. Fitted Microscopic Thermodynamic Parameters for $[Ln_2(\mathbf{L}k)_n]^{6+}$ ($k = 7, 8$; $n = 1, 2$) by Using Eqs 5, 6, and 13-15 (Ln = La, Eu, Y, Lu; CH_2Cl_2/CH_3CN 1:1, 298 K)[a]

fitted params	La	Eu	Y	Lu
First Fit with Ligands **L7** and **L9**: f^{Ln}_{N2O}, $EM^{Ln,\mathbf{L7}}_{double}$, $u^{N2O,N2O}$, $u^{Ln,Ln}_{\mathbf{L7}}$				
log (f^{Ln}_{N2O})	6.7(1)	7.2(2)	7.1(1)	6.8(1)
$\Delta G^{Ln,N2O}_{inter}$/kJ mol^{-1} [b]	−38.4(7)	−41(1)	−40.4(3)	−39.0(7)
log $EM^{Ln,\mathbf{L7}}_{double}$	−6.3(3)	−5.5(4)	−6.2(1)	−5.5(3)
$\Delta G^{Ln,\mathbf{L7}}_{intra}$/kJ mol^{-1} [c]	−3(1)	−10(2)	−5.1(6)	−8(1)
log $u^{N2O,N2O}$	−0.2(1)	−0.5(2)	0.12(6)	0.1(1)
$\Delta E^{N2O,N2O}$/kJ mol^{-1} [d]	0.9(8)	3(1)	−0.6(3)	−0.3(8)
log $u^{Ln,Ln}_{\mathbf{L7}}$	−3.5(3)	−5.0(5)	−4.5(1)	−4.2(3)
$\Delta E^{Ln,Ln}_{\mathbf{L7}}$/kJ mol^{-1} [e]	20(2)	29(3)	26(1)	24(2)
Second Fit with Ligands **L8** and **L10**: f^{Ln}_{N3}, $EM^{Ln,\mathbf{L8}}_{double}$, $u^{N3,N3}$, $u^{Ln,Ln}_{\mathbf{L8}}$				
log f^{Ln}_{N3}	6.9(2)	6.8(2)	6.6(1)	7.35(3)
$\Delta G^{Ln,N3}_{inter}$/kJ mol^{-1} [b]	−39(1)	−39(1)	−37.7(6)	−41.9(2)
log $EM^{Ln,\mathbf{L8}}_{double}$	−8.0(4)	−7.5(4)	−7.4(3)	−6.6(1)
$\Delta G^{Ln,\mathbf{L8}}_{intra}$/kJ mol^{-1} [c]	6(1)	4(2)	5(2)	−4.4(5)
log $u^{N3,N3}$	−0.2(1)	−0.4(2)	−0.3(2)	−1.12(4)
$\Delta E^{N3,N3}$/kJ mol^{-1} [d]	1(1)	2(1)	2(1)	6.4(2)
log $u^{Ln,Ln}_{\mathbf{L8}}$	−3.5(4)	−4.3(5)	−2.9(3)	−5.1(1)
$\Delta E^{Ln,Ln}_{\mathbf{L8}}$/kJ mol^{-1} [e]	20(2)	25(3)	17(2)	28.9(5)

[a] The uncertainties correspond to those found during the multilinear least-squares fits. [b] $\Delta G^{Ln,N2O}_{intra} = -RT \ln (f^{Ln}_{N2O})$ and $\Delta G^{Ln,N3}_{inter} = -RT \ln (f^{Ln}_{N3})$. [c] $\Delta G^{Ln,\mathbf{L}k}_{inter} = -RT \ln(f^{Ln}_{\mathbf{L}k} EM^{Ln,\mathbf{L}k}_{double})$. [d] $\Delta E^{\mathbf{L}k,\mathbf{L}k} = -RT \ln(u^{\mathbf{L}k,\mathbf{L}k})$. [e] $\Delta E^{Ln,Ln}_{\mathbf{L}k} = -RT \ln(u^{Ln,Ln}_{\mathbf{L}k})$.

(37) The statistical factors for eqs (10)-(12) are derived in ref 16, and those for eqs (13)-(15) can be found in ref 20.

(38) Le Borgne, T.; Altmann, P.; André, N.; Bünzli, J.-C. G.; Bernardinelli, G.; Morgantini, P.-Y.; Weber, J.; Piguet, C. *Dalton Trans.* **2004**, 723–733.

(39) Willcott, M. R.; Lenkinski, R. E.; Davis, R. E. *J. Am. Chem. Soc.* **1972**, *94*, 1742–1744. $AF_{Ln} = \{[\sum_i(\log \beta^{Ln,L}_{i,exp} - \log \beta^{Ln,L}_{i,calcd})^2]/[\sum_i(\log \beta^{Ln,L}_{i,exp})^2]\}^{1/2}$.

(40) Dalla Favera, N.; Kiehne, U.; Bunzen, J.; Hytteballe, S.; Lützen, A.; Piguet, C. *Angew. Chem., Int. Ed.* DOI: 10.1002/anie.200904614.

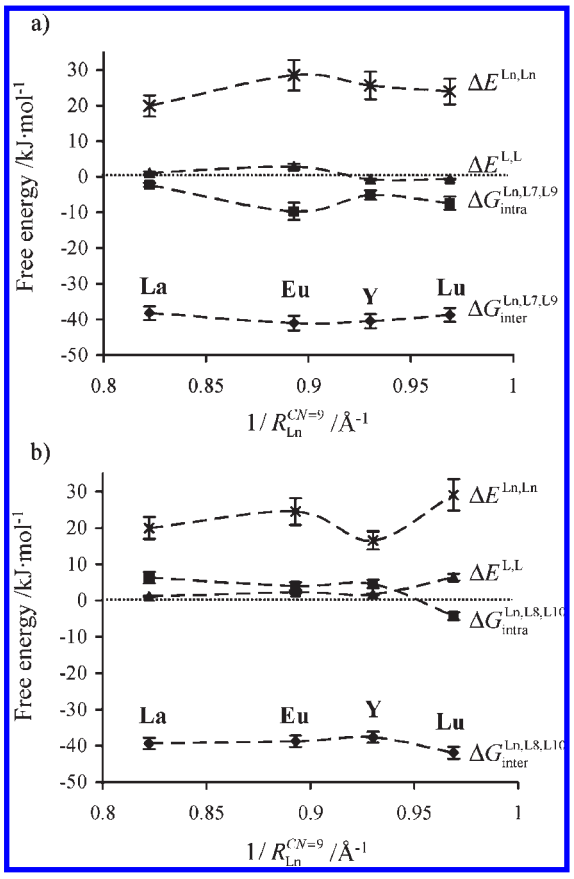

Figure 5. Plots of the four microscopic thermodynamic parameters in the form of free energies of interactions, in function of the inverse of nine-coordinate ionic radii for the assemblies of (a) $[Ln(\mathbf{L9})_n]^{3+}$ and $[Ln_2(\mathbf{L7})_p]^{6+}$ and (b) $[Ln(\mathbf{L10})_n]^{3+}$ and $[Ln_2(\mathbf{L8})_p]^{6+}$ ($n = 1-3$, $p = 1$, 2, 1:1 CH_2Cl_2/CH_3CN, 298 K). The dotted lines are only guides for the eyes.

$(f^{Ln}_{N2O}EM^{Ln,\mathbf{L7}}_{double}) \leq -3$ kJ mol^{-1}; Figure 5a) but globally unfavorable for the N_3 binding units ($-4 \leq \Delta G^{Ln,\mathbf{L8}}_{intra} = -RT\ln(f^{Ln}_{N3}EM^{Ln,\mathbf{L8}}_{double}) \leq +6$ kJ mol^{-1}; Figure 5b).

Once the microscopic thermodynamic parameters are at hand (Table 2), the stability of the missing saturated triple-stranded complexes $[Ln_2(\mathbf{L}k)_3]^{6+}$ ($k = 7$, 8, equilibrium 16) can be computed *a posteriori* with eq 17 (the statistical factors is calculated in Figure S13, Supporting Information).

$$3\mathbf{L}k + 2[Ln(CH_3CN)_9]^{3+} \rightleftharpoons [Ln_2(\mathbf{L}k)_3]^{6+} + 18CH_3CN \quad \beta^{Ln,\mathbf{L}k}_{2,3} \qquad (16)$$

$$\beta^{Ln,\mathbf{L}k}_{2,3} = 96(f^{Ln}_{\mathbf{L}k})^6(u^{\mathbf{L}k,\mathbf{L}k})^6(u^{Ln,Ln}_{\mathbf{L}k})(c^{eff,\mathbf{L}k}_{double})(c^{eff,\mathbf{L}k}_{triple}) \qquad (17)$$

As a first approximation, we can tentatively assume that the effective molarities for macrocyclization (i.e., transforming the single-stranded helicate $[Ln_2(\mathbf{L}k)]^{6+}$ into the double-stranded helicate $[Ln_2(\mathbf{L}k)_2]^{6+}$, $EM^{Ln,\mathbf{L}k}_{double}$) and for macrobicyclization (i.e., transforming the double-stranded helicate $[Ln_2(\mathbf{L}k)_2]^{6+}$ into the triple-stranded helicate $[Ln_2(\mathbf{L}k)_3]^{6+}$, $EM^{Ln,\mathbf{L}k}_{triple}$) are comparable: $EM^{Ln,\mathbf{L}k}_{triple} \approx EM^{Ln,\mathbf{L}k}_{double}$ (Table 3, entries 1 and 5). The introduction of the microscopic parameters of Table 2 into eq 17 thus predicts $25.4 \leq \log\beta^{Ln,\mathbf{L7}}_{2,3} \leq 28.3$ (Table 3, entry 2) and $21.2 \leq \log\beta^{Ln,\mathbf{L8}}_{2,3} \leq 23.0$ (Table 3, entry 6), which should result in the almost quantitative formation of the saturated triple-stranded helicate (for Ln: La, Eu, Y, Lu; $\mathbf{L}k = 2{:}3$) during ^{1}H NMR titration performed at 10^{-2} M (Figure 6a and Figure S14a, Supporting Information), in complete disagreement with experimental data (Figures S4−S7 and S9, Supporting Information). Our tentative hypothesis is thus wrong, and the origin of this discrepancy can be assigned to $EM^{Ln,\mathbf{L}k}_{triple} \ll EM^{Ln,\mathbf{L}k}_{double}$,[41] which prevents the

Table 3. Values of $\log\beta^{Ln,\mathbf{L}k}_{2,3}$ and $\log EM^{Ln,\mathbf{L}k}_{triple}$ for the Virtual Triple-Stranded Complexes $[Ln_2(\mathbf{L}k)_3]^{6+}$ ($k = 7$, 8) Computed by Using Eq 17 (Ln = La, Eu, Y, Lu; 1:1 CH_2Cl_2/CH_3CN, 298 K)

computed params	La	Eu	Y	Lu
Ligand **L7**: N_2O Binding Units				
$\log EM^{Ln,\mathbf{L7}}_{triple} \approx \log EM^{Ln,\mathbf{L7}}_{double}$ [a]	−6.3	−5.5	−6.2	−5.5
$\log\beta^{Ln,\mathbf{L7}}_{2,3,calcd}$ [b]	24.9	26.2	28.4	28.2
$\log\beta^{Ln,\mathbf{L7}}_{2,3,max}$ [c]	19.9	20.6	20.9	20.8
$\log EM^{Ln,\mathbf{L7}}_{triple}$ [b]	−11.3	−11.1	−13.7	−12.9
Ligand **L8**: N_3 Binding Units				
$\log EM^{Ln,\mathbf{L8}}_{double} \approx \log EM^{Ln,\mathbf{L8}}_{triple}$ [a]	−8.0	−7.5	−7.4	−6.6
$\log\beta^{Ln,\mathbf{L8}}_{2,3,calcd}$ [b]	22.7	21.1	22.1	21.1
$\log\beta^{Ln,\mathbf{L8}}_{2,3,max}$ [c]	19.0	17.9	18.4	18.6
$\log EM^{Ln,\mathbf{L7}}_{triple}$ [b]	−11.7	−10.7	−11.1	−9.1

[a] Taken from Table 2. [b] Computed with eq 17 and data given in the previous row. [c] Maximium values estimated by using nonlinear least-squares simulation of the ligand speciation with the condition that the quantities of $[Ln_2(\mathbf{L}k)_3]^{6+}$ ($k = 7$, 8) in solution never exceed 5% of the ligand speciation for $|\mathbf{L}k|_{tot} = 10^{-2}$ M (see text and Figure 6b).

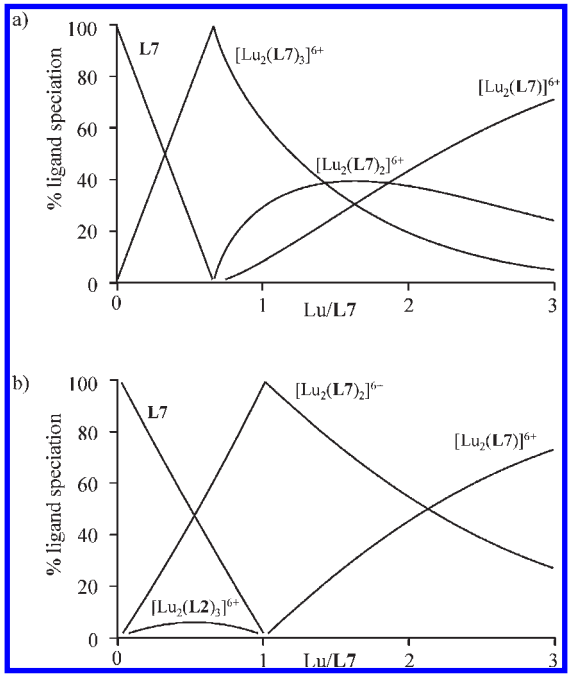

Figure 6. Theoretical ligand speciation for the titration of **L7** (10^{-2} M in 1:1 CH_2Cl_2/CD_3CN) with $Lu(CF_3SO_3)_3\cdot 4H_2O$: (a) computed by using $\log\beta^{Ln,\mathbf{L7}}_{2,3}$ estimated with $EM^{\mathbf{L7}}_{triple} \approx EM^{\mathbf{L7}}_{double}$ (Table 2, entries 1 and 2); (b) computed by using $\beta^{Ln,\mathbf{L7}}_{2,3}$ estimated with $EM^{\mathbf{L7}}_{triple} \ll EM^{\mathbf{L7}}_{double}$ (Table 3, entries 3 and 4).

(41) In agreement with its definition in the site binding model,[1] $\Delta E^{L,L}$ is restricted to operate within the coordination sphere of a single metal, and its value thus does not depend on nuclearity. Moreover, $\Delta E^{L,L}$ is relatively insensitive to the number of N_2O[9a,38] or N_3[9a] tridentate binding sites connected to Ln(III), and it is therefore safe to assign the global destabilization of the triple-stranded complexes to $EM^{Ln,\mathbf{L}k}_{triple} \ll EM^{Ln,\mathbf{L}k}_{double}$.

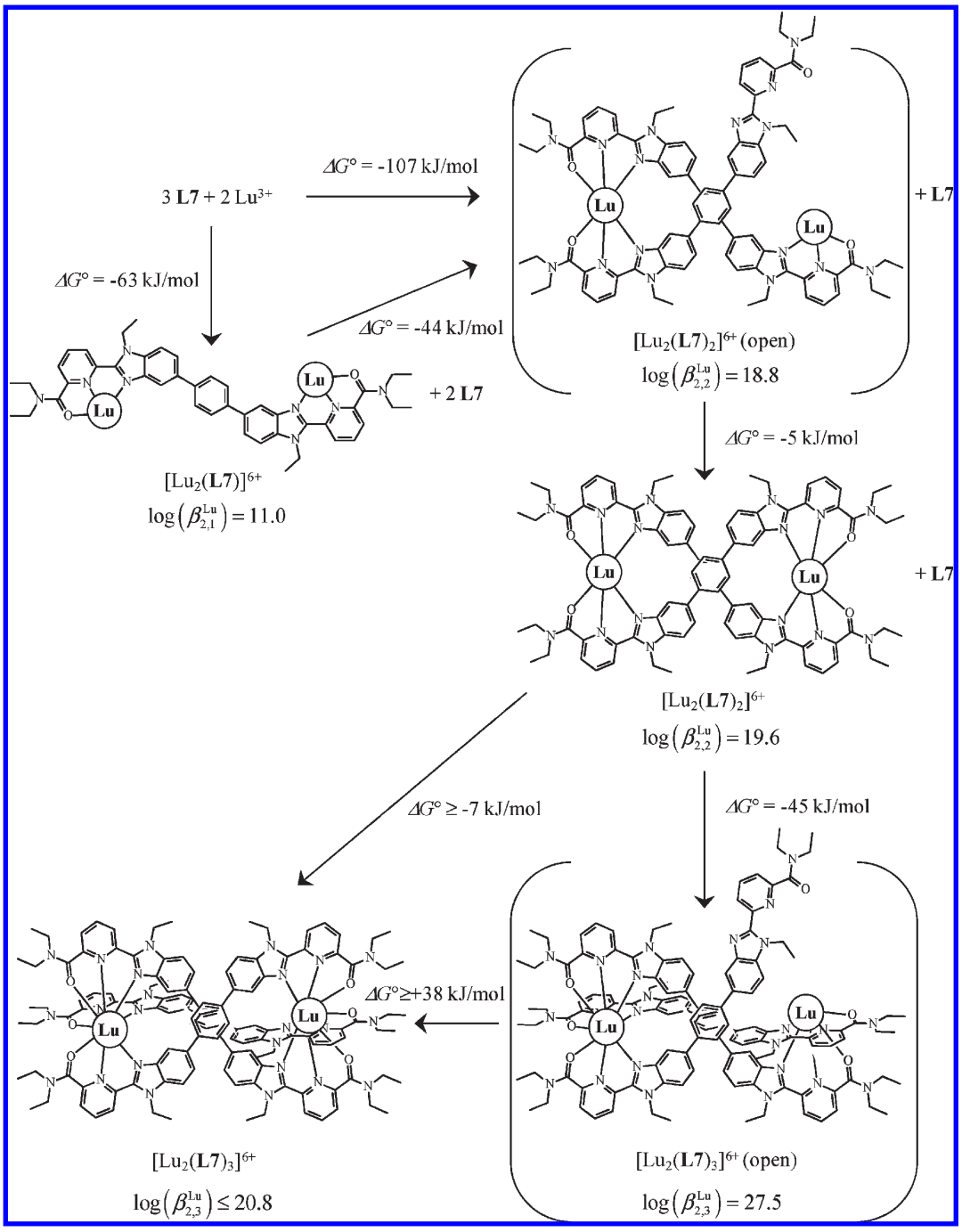

Figure 7. Dissection of the thermodynamic self-assembly of $[Lu_2(\mathbf{L7})_2]^{6+}$ computed with the microscopic thermodynamic parameters of Tables 2 and 3. The stability constants calculated for the open structures shown in brackets are only indicative, because these complexes are not detected under thermodynamic equilibrium, but they highlight the tragic consequences of the intramolecular macrocyclization processes with this constrained ligand.

second intramolecular connection process to occur (i.e., the transformation of the double-stranded complexes into the triple-stranded helicates, Figure 7 and Figure S15, Supporting Information). Fixing a reasonable minimum limit for the ^{1}H NMR detection of $[Ln_2(\mathbf{L}k)_3]^{6+}$ to 5% of the ligand speciation, we can estimate $21.2 \leq \log \beta_{2,3}^{Ln,\mathbf{L7}} \leq 23.0$ (Table 3, entry 3) and $17.9 \leq \log \beta_{2,3}^{Ln,\mathbf{L8}} \leq 19.0$ (Table 3, entry 7) by using nonlinear least-squares simulation of the ligand speciation in solution (Figure 6b and Figure S14b, Supporting Information), from which $10^{-13.7} \leq EM_{triple}^{Ln,\mathbf{L7}} \leq 10^{-11.1}$ M and $10^{-11.7} \leq EM_{triple}^{Ln,\mathbf{L8}} \leq 10^{-9.1}$ M can be calculated with eq 17 (Table 3, entries 4 and 8). The decrease by 3−6 orders of magnitude on going from $EM_{double}^{Ln,\mathbf{L}k}$ to $EM_{triple}^{Ln,\mathbf{L}k}$ is diagnostic for drastic enthalpic constraints originating from steric limitations encountered during ring closure, which eventually prevent the successive macrocyclization processes required for the formation of multiple-stranded helicates (Figure 7 and Figure S15, Supporting Information).

The Ultimate Pieces of the Puzzle: Isolation and Structures of Double-Stranded Helicates in the Solid State. According to the speciations observed by ^{1}H NMR for titration of **L7** (Figure S12, Supporting Information) and **L8** (Figure S11, Supporting Information) at high concentrations (i.e., $|\mathbf{L}k|_{tot} = 10$ mM), the isolation of pure

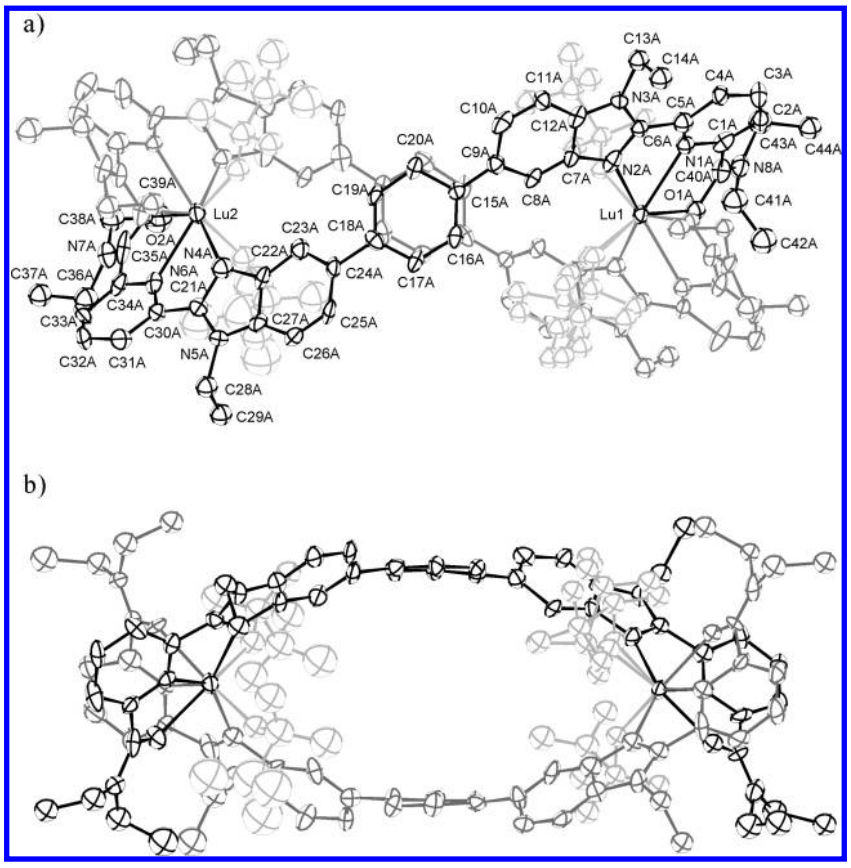

Figure 8. Perspective views perpendicular to the helical axis with numbering scheme of the molecular structure of the double-stranded cation $[Lu_2(\mathbf{L7})_2(CF_3SO_3)_4]^{2+}$ in the crystal structure of **6**. Ellipsoids are represented at the 30% probability level. Strand A is shown in black, strand B in heavy gray, and coordinated triflates in light gray.

double-stranded helicates $[Ln_2(\mathbf{L}k)_2]^{6+}$ for Ln:**L***k* = 1.0 is straightforward (yields 30−75%), as confirmed by the elemental analyses of the microcrystalline powders of $[Ln_2(\mathbf{L}k)_2](CF_3SO_3)_6 \cdot xH_2O$ (Ln = La, Eu, Lu, Y ; k = 7, 8; x = 4−13; Table S5, Supporting Information). However, the observed mixtures of double-stranded $[Ln_2(\mathbf{L}k)_2]^{6+}$ and single-stranded $[Ln_2(\mathbf{L}k)]^{6+}$ for Ln:**L***k* = 2.0 (Figures S11 and S12, Supporting Information) prevent the isolation of pure 2:1 complexes in the solid state with **L7** (Table S5, Supporting Information). For **L8**, the minute effective molarities sufficiently destabilize the formation of the macrocyclic double-stranded helicates (Table 2), thus allowing the isolation of pure noncyclic single-stranded complexes $[Ln_2(\mathbf{L8})](CF_3SO_3)_6 \cdot xH_2O$ (Ln:**L***k* = 2.0) with the small lanthanides (Ln = Y, Lu). For the larger metals (Ln = La, Eu), contamination with 10−20% of $[Ln_2(\mathbf{L8})_2](CF_3SO_3)_6 \cdot xH_2O$ is unavoidable (Table S5, Supporting Information). Slow diffusion of *tert*-butyl methyl ether into a concentrated solution of $[Lu_2(\mathbf{L7})_2](CF_3SO_3)_6$ in acetonitrile gives fragile yellow X-ray-quality crystals of $[Lu_2(\mathbf{L7})_2](CF_3SO_3)_4](CF_3SO_3)_2 \cdot CH_3CN \cdot 3H_2O$ (**6**). Due to the limited quality of the diffraction data (see the Experimental Section), we focus here on the shape and on the global metric of the binuclear double-stranded helical cation $[Lu_2(\mathbf{L7})_2(CF_3SO_3)_4]^{2+}$, the solvent molecules and the two remaining ionic triflate anions being disordered. In agreement with ^{1}H NMR data recorded in solution, the molecular structure of the cation shows the two ligands wrapped about a pseudo-2-fold axis passing through the two octa-coordinate Lu(III) atoms (Figure 8). The Lu···Lu intrahelical distance of 13.26(2) Å greatly exceeds the 9.06(3) Å reported for the intermetallic separation in the triple-stranded helicate $[Tb_2(\mathbf{L1})_3]^{6+}$ and 9.05(3) Å found in the double-stranded side-by-side complex $[Eu_2(\mathbf{L1})_2(CF_3SO_3)_4(H_2O)_2]^{2+}$.[42] This corresponds to a logical extension due to the replacement of the compact twisted methylene spacer in **L1**, with the larger linear *p*-phenyl in **L7**.

The main torsions in the ligand strands result from rotation about the interannular C−C bonds connecting the aromatic benzimidazole and phenyl rings, which are obtained at the expense of a reduced overlap between the aromatic π systems (interplanar angles = 33−42°; Table S6, Supporting Information). The helical arrangement of the two wrapped ligands thus produces a prolate ellipsoidal intermetallic cavity (occupied by one disordered water molecule; see the Experimental Section), with its long axis passing through the Lu atoms, while its short axis could be defined by the separation between the two central phenyl rings of the spacers (interplanar angle 7.2°, average interplanar distance 6.9 Å; Table S6, Supporting Information). The geometrical characteristics of the double-stranded helix $[Lu_2(\mathbf{L7})_2(CF_3SO_3)_4]^{2+}$ (total length L = 20.3 Å for a total rotation of 1.15 turn, pitch P = 17.7 Å/turn) are significantly different from those observed for the analogous, but triple-stranded helix $[Tb_2(\mathbf{L1})_3]^{6+}$ (total length L = 11.9 Å for a total rotation of 0.81 turn, pitch P = 14.7 Å/turn).[42] However, we do

(42) Martin, N.; Bünzli, J.-C. G.; McKee, V.; Piguet, C.; Hopfgartner, G. *Inorg. Chem.* **1998**, *37*, 577–589.

not detect strong constraints in the metallic coordination sphere, each Lu(III) atom being eight-coordinated by two tridentate N_2O binding units and by two monodentate triflate anions, thus forming slightly distorted dodecahedrons (Figure 8). The Lu−N and Lu−O bond lengths are standard (Table S6, Supporting Information), leading to ionic radii of $R_{Lu1}^{CN=8} = 0.97$ Å and $R_{Lu2}^{CN=8} = 0.96$ Å, which are close to the expected value for nonconstrained Lu(III) (0.977 Å).[43]

Conclusion

Inspired by the unusual crystal structures of lanthanide complexes with **L5**[18] and **L6**,[19] in which the first coordination spheres are not saturated with tridentate binding units, we deliberately designed ligands **L7** and **L8** for investigating the thermodynamic parameters responsible for significant deviations from the principle of maximum site occupancy. The effective molarity EM, which contains both the enthalpic and entropic corrections required for transforming an intermolecular connection into its intramolecular counterpart ($EM = e^{(\Delta G_{inter}^{M,L\boldsymbol{k}} - \Delta G_{intra}^{M,L\boldsymbol{k}})/RT}$),[3] indeed controls the number of favorable macrocyclization processes leading to stable oligomeric complexes. In **L7** and **L8**, the rigid para-disubstituted phenyl spacer produces values for the effective molarities ($EM_{double}^{Ln,L\boldsymbol{k}} = 10^{-8}-10^{-6}$ M, $EM_{triple}^{Ln,L\boldsymbol{k}} = 10^{-13}-10^{-9}$ M) so low that intramolecular connections (($\Delta G_{intra}^{Ln,L\boldsymbol{k}} = \Delta G_{inter}^{Ln,L\boldsymbol{k}} - RT \ln (EM^{Ln,L\boldsymbol{k}})$) computed for standard state 1 M) are only compatible with a single macrocyclization process and the assembly of the double-stranded helicates $[Ln_2(L\boldsymbol{k})_2]^{6+}$ (k = 7, 8). The total lack of the triple-stranded helicates $[Ln_2(L\boldsymbol{k})_3]^{6+}$ in solution, which however simultaneously satisfy the principle of maximum site occupancy and the principle of stereochemical matching, can be thus eventually explained by the large decrease of EM for the second macrocyclization process ($EM_{triple}^{Ln,L\boldsymbol{k}} \ll EM_{double}^{Ln,L\boldsymbol{k}}$). This phenomenon is probably at the origin of the discovery of several unexpected and often aesthetically appealing structures by serendipity, when constrained ligands with restricted degrees of freedoms are considered.[8,19] Our results suggest that, except for some kinetically controlled interfaces of crystallization, which escape a thermodynamic rationalization, the manipulation and tuning of the effective molarities in coordination and supramolecular chemistry can be rationally exploited for better predicting the output of self-assembly processes without relying on chance and on statistics. As far as short-term applications are concerned, the deliberate design of systems displaying low values of EM are attractive for the preparation of stable single-stranded polynuclear lanthanide oligomers or polymers, for which the associated intermolecular complexation processes are easily amenable to thermodynamic modeling[9b] and predictions[51] and to deliberate metal selection[52] for the design of pure heterometallic f−f′ luminescent complexes.[53]

Experimental Section

Chemicals were purchased from Fluka AG and Aldrich and used without further purification unless otherwise stated. The syntheses of the starting synthons **1** and **2** (Scheme 2) are described in the Supporting Information (Scheme S3). The ligands **L9**[38] and **L10**[32] were prepared according to literature procedures. The trifluoromethanesulfonate salts $Ln(CF_3SO_3)_3 \cdot xH_2O$ were prepared from the corresponding oxide (Aldrich, 99.99%).[44] The Ln content of the solid salt was determined by complexometric titrations with Titriplex III (Merck) in the presence of urotropine and xylene orange.[45] Acetonitrile and dichloromethane were distilled over calcium hydride. Silica gel plates Merck 60 F_{254} were used for thin-layer chromatography (TLC), and Fluka silica gel 60 (0.04−0.063 mm) or Acros neutral activated alumina (0.050−0.200 mm) was used for preparative column chromatography.

Preparation of 3. To a cooled (0 °C, ice bath) 30 mL chloroform solution containing **1** (1.26 g, 3.73 mmol) and K_2CO_3 (0.77 g, 5.6 mmol) was slowly added phenyltriflimide (Ø-N$(Tf)_2$, 1.89 g, 5.48 mmol) in chloroform (40 mL) under an inert atmosphere. The resulting mixture was then refluxed for 20 h, diluted with dichloromethane (150 mL), and washed with aqueous half-saturated NH_4Cl (200 mL). The separated organic layer was dried (Na_2SO_4) and filtered and the solvent removed under reduced pressure to give a dark brown oil. The crude material was then purified by column chromatography (silica gel, 98:2 CH_2Cl_2/CH_3OH) to give **3** as a yellow viscous oil (1.73 g, 3.69 mmol, yield 99%). ^{1}H NMR ($CDCl_3$; 400 MHz): δ 1.06 (t, ^3J = 7 Hz, 3H), 1.27 (t, ^3J = 7 Hz, 3H), 1.47 (t, ^3J = 7 Hz, 3H), 3.33 (q, ^3J = 7 Hz, 2H), 3.60 (q, ^3J = 7 Hz, 2H), 4.77 (q, ^3J = 7 Hz, 2H), 7.26 (dd, ^3J = 9 Hz, ^4J = 2.4 Hz, 1H), 7.8 (d, ^3J = 9 Hz, 1H), 7.57 (d, ^3J = 8 Hz, 1H), 7.74 (d, ^4J = 2 Hz, 1H), 7.97 (t, ^3J = 8 Hz, 1H), 8.38 (d, ^3J = 8 Hz, 1H). ESI-MS: m/z 470.5 ($[M + H]^+$), 941.7 ($[2M + H]^+$).

Preparation of 4. To a cooled (0 °C, ice bath) 50 mL chloroform solution containing **2** (3.0 g, 7.8 mmol) and K_2CO_3 (1.52 g, 11.0 mmol) was slowly added phenyltriflimide (Ø-N$(Tf)_2$, 3.9 g, 10.9 mmol) in chloroform (25 mL) under an inert atmosphere. The resulting mixture was then refluxed for 6 h, diluted with dichloromethane (300 mL), and washed with aqueous half-saturated NH_4Cl (200 mL). The separated organic layer was dried (Na_2SO_4) and filtered and the solvent removed under reduced pressure to give a pale yellow oil. The crude material was then purified by column chromatography (silica gel, 100:0 → 99:1 CH_2Cl_2/CH_3OH) to give **4** as a yellow viscous oil (4.0 g, 7.8 mmol, yield 100%). ^{1}H NMR ($CDCl_3$; 400 MHz): δ 1.39 (t, ^3J = 7 Hz, 3H), 1.40 (t, ^3J = 7 Hz, 3H), 4.80 (q, ^3J = 7 Hz, 2H), 4.83 (q, ^3J = 7 Hz, 2H), 7.31 (dd, ^3J = 9 Hz, ^4J = 2 Hz, 1H), 7.37 (t, ^3J = 7 Hz, 1H), 7.40 (t, ^3J = 7 Hz, 1H), 7.50 (d, ^3J = 9 Hz, 1H), 7.52 (d, ^3J = 9 Hz, 1H), 7.80 (d, ^4J = 2 Hz, 1H), 7.89 (d, ^3J = 8 Hz, 1H), 8.09 (t, ^3J = 8 Hz, 1H), 8.35 (d, ^3J = 8 Hz, 1H), 8.40 (d, ^3J = 8 Hz, 1H). ESI-MS: m/z 516.5 ($[M + H]^+$), 1031.6 ($[2M + H]^+$).

Preparation of 5. A 20 mL THF solution of 1,4-dibromobenzene (4.72 g, 20 mmol) was added dropwise to a suspension of magnesium shavings (1.06 g, 43.6 mmol) in dry THF (10 mL) under an inert atmosphere. The mixture was refluxed for 24−48 h until a gray precipitate appeared. Trimethylborate (5 mL, 4.66 g, 44.8 mmol) in THF (50 mL) was added and the mixture refluxed for 2 h. The white gel was poured onto aqueous hydrochloric acid (2 M, 200 mL) and stirred for 1 h at room temperature. The clear solution was extracted with diethyl ether (4 × 200 mL), and the combined organic phases were dried (Na_2SO_4), filtered, and evaporated to dryness. Recrystallization from hot water (200 mL) gave **5** as transparent crystals (1.6 g, 9.6 mmol, 48%). ^{1}H NMR (d_6-acetone; 400 MHz): δ 7.86 (s, 4H), 7.13 (s, 4H). ESI-MS (negative mode/CH_3OH): m/z 165.3 ($[M - H]^-$).

Preparation of L7. Compounds **3** (0.94 g, 2.0 mmol) and **5** (166 mg, 1.0 mmol) were dissolved in degazed dioxane/ethanol (30 mL/20 mL) containing cesium fluoride (610 mg, 4.0 mmol)

(43) Shannon, R. D. *Acta Crystallogr.* **1976**, *A32*, 751–767.

(44) Desreux, J. F. In *Lanthanide Probes in Life, Chemical and Earth Sciences*; Bünzli, J.-C. G., Choppin, G. R., Eds.; Elsevier: Amsterdam, 1989; Chapter 2.

(45) Schwarzenbach, G. *Complexometric Titrations*; Chapman & Hall: London, 1957; p 8.

under an inert atmosphere. The $Pd(PPh_3)_4$ catalyst (100 mg, 0.09 mmol was added, and the resulting dark solution was stirred for 20 min at room temperature and finally refluxed for 24 h. After evaporation to dryness, the solid residue was partitioned between dichloromethane and aqueous half-saturated NaCl (150 mL/200 mL). The aqueous phase was separated and extracted with dichloromethane (200 mL), and the combined organic phases were dried (Na_2SO_4), filtered, and evaporated to dryness. The crude brown solid was purified by column chromatography (silica gel, 99.5:0:0.5 → 96.5:3:0.5 $CH_2Cl_2/CH_3OH/NEt_3$) to give a pale yellow solid, which was recrystallized from dichloromethane/methanol to eventually provide **L7** as a microcrystalline yellow powder (0.5 g, 0.68 mmol, yield 68%). ^{1}H NMR ($CDCl_3$; 400 MHz): δ 1.08 (t, ^3J = 7.1 Hz, 6H), 1.29 (t, ^3J = 7.1 Hz, 6H), 1.51 (t, ^3J = 7.1 Hz, 6H), 3.36 (q, ^3J = 7.1 Hz, 4H), 3.62 (q, ^3J = 7.1 Hz, 4H), 4.80 (q, ^3J = 7.1 Hz, 4H), 7.53 (d, ^3J = 8.6 Hz, 2H), 7.56 (d, ^3J = 8.0 Hz, 2H), 7.67 (d, ^3J = 8.2 Hz, 2H), 7.78 (s, 4H), 7.96 (t, ^3J = 7.9 Hz, 2H), 8.12 (s, 2H), 8.44 (d, ^3J = 7.9 Hz, 2H). ESI-MS: m/z 360.6 ([**L7** + 2H]$^{2+}$), 719.8 ([**L7** + H]$^+$). Anal. Calcd for $C_{44}H_{46}N_8O_2 \cdot H_2O$: C, 71.71; H, 6.57; N, 15.20. Found: C, 71.75; H, 6.30; N, 14.80.

Preparation of L8. Compounds **4** (1.3 g, 2.61 mmol) and **5** (216 mg, 1.30 mmol) were dissolved in degazed dioxane/ethanol (30 mL/20 mL) containing cesium fluoride (1 g, 6.58 mmol) under an inert atmosphere. The $Pd(PPh_3)_4$ catalyst (150 mg, 0.13 mmol) was added, and the resulting dark solution was stirred for 20 min at room temperature and finally refluxed for 4 h. After evaporation to dryness, the solid residue was partitioned between dichloromethane and aqueous half-saturated NaCl (150 mL/200 mL). The aqueous phase was separated and extracted with dichloromethane (200 mL), and the combined organic phases were dried (Na_2SO_4), filtered, and evaporated to dryness. The crude brown solid was purified by column chromatography (silica gel, 99.5:0:0.5 → 96.5:3:0.5 $CH_2Cl_2/CH_3OH/NEt_3$) to give a pale yellow solid, which was recrystallized from dichloromethane/methanol to eventually provide **L8** as a microcrystalline yellow powder (0.76 g, 0.92 mmol, yield 70%). X-ray-quality prisms of **L8**·3$CHCl_3$ were obtained by slow diffusion of hexane into a concentrated solution of **L8** in chloroform at room temperature. ^{1}H NMR ($CDCl_3$; 400 MHz): δ 1.40 (t, ^3J = 7 Hz, 3H), 1.42 (t, ^3J = 7 Hz, 3H), 4.83 (q, ^3J = 7 Hz, 2H), 4.85 (q, ^3J = 7 Hz, 2H), 7.38 (multiplet, 4H), 7.51 (dd, ^3J = 6 Hz, ^4J = 2 Hz, 2H), 7.58 (d, ^3J = 8 Hz, 2H), 7.72 (dd, ^3J = 7 Hz, ^4J = 1 Hz, 2H), 7.83 (s, 4H), 7.91 (dd, ^3J = 7 Hz, ^4J = 1 Hz, 2H), 8.10 (t, ^3J = 7 Hz, 2H), 8.18 (d, ^4J = 1 Hz, 2H), 8.39 (d, ^3J = 8 Hz, 2H), 8.41 (d, ^3J = 8 Hz, 2H). ESI-MS: m/z 405.5 ([**L8** + 2H]$^{2+}$), 810 ([**L8** + H]$^+$). Anal. Calcd for $C_{52}H_{44}N_{10} \cdot H_2O$: C, 75.52; H 5.60; N, 16.94. Found: C, 75.60; H, 5.47; N, 16.72.

Preparation of the Complexes $[Ln_2(L\mathit{k})_2](CF_3SO_3)_6$ and $[Ln_2(L\mathit{k})](CF_3SO_3)_6$ (k = 7, 8; Ln = La, Eu, Lu, Y). To a 1 mL chloroform solution of **L*k*** (k = 7, 8; 28 μmol, 1 equiv) was added $Ln(CF_3SO_3)_3 \cdot xH_2O$ (x = 4, 5; 28 μmol for 2:2 complexes and 56 μmol for 2:1 complexes) in acetonitrile (1 mL). The resulting clear solutions were stirred for 1 h and filtered, and microscrytalline powders were deposited upon slow diffusion of diethyl ether. The resulting solids were collected by filtration and dried in vacuo to give $[Ln_2(L\mathit{k})_2](CF_3SO_3)_6 \cdot xH_2O$ and $[Ln_2(L\mathit{k})](CF_3SO_3)_6 \cdot xH_2O$ in 30−75% yields (x = 1−13; Table S5, Supporting Information). X-ray-quality prisms of $[Lu_2(\mathbf{L7})_2](CF_3SO_3)_6 \cdot CH_3CN \cdot 3H_2O$ (**6**) were obtained by slow diffusion of *tert*-butyl methyl ether vapors into a concentrated solution of the complex in acetonitrile.

Spectroscopic Measurements. Spectrophotometric titrations were performed with a J&M diode array spectrometer (Tidas series) connected to an external computer. In a typical experiment, 50 mL of ligand in 1:1 CH_2Cl_2/CH_3CN (10^{-4} M) was titrated at 298 K with a solution of $Ln(Otf)_3 \cdot xH_2O$ (10^{-3} M) in 1:1 CH_2Cl_2/CH_3CN under an inert atmosphere. After each addition of 0.20 mL, the absorbance was recorded using Hellma optrodes (optical path length 0.1 cm) immersed in the thermostated titration vessel and connected to the spectrometer. Mathematical treatment of the spectrophotometric titrations was performed with factor analysis[33] and with the SPECFIT program.[34] ^{1}H, ^{19}F, and ^{13}C NMR spectra were recorded at 298 K on Bruker Avance 400 MHz and Bruker DRX 500 MHz spectrometers. Chemical shifts are given in ppm with respect to TMS. Pneumatically assisted electrospray (ESI-MS) mass spectra were recorded from 10^{-4} M solutions on an Applied Biosystems API 150EX LC/MS system equipped with a Turbo Ionspray source. Least-squares fits were performed with Excel. Elemental analyses were performed by Dr. H. Eder from the Microchemical Laboratory of the University of Geneva.

X-ray Crystallography. A summary of crystal data, intensity measurements, and structure refinements for **S6**, **L8**·3$CHCl_3$, and $[Lu_2(\mathbf{L7})_2](CF_3SO_3)_6 \cdot CH_3CN \cdot 3H_2O$ (**6**) are collected in Table S7 (Supporting Information). All crystals were mounted on quartz fibers with protection oil. Cell dimensions and intensities were measured at 150 K on a Stoe IPDS diffractometer with graphite-monochromated Mo Kα radiation (λ = 0.710 73 Å). Data were corrected for Lorentz and polarization effects and for absorption. The structures were solved by direct methods (SIR97);[46] all other calculations were performed with ShelX97 (**L8**·3$CHCl_3$ and **6**),[47] XTAL (**S6**)[48] systems, and ORTEP[49] programs. CCDC-753961 and 753962 contain the supplementary crystallographic data for **S6** and **L8**·3$CHCl_3$, respectively. The CIF files can be obtained free of charge via www.ccdc.cam.ac.uk/conts/retrieving.html (or from the Cambridge Crystallographic Data Centre, 12 Union Road, Cambridge CB2 1EZ, U.K.; fax (+ 44) 1223-336-033, e-mail deposit@ccdc.cam.ac.uk). The CIF file of $[Lu_2(\mathbf{L7})_2](CF_3SO_3)_6 \cdot CH_3CN \cdot 3H_2O$ (**6**) is given in the Supporting Information.

Comments on the Crystal Structure of S6. All non-hydrogen atoms (20) were refined with anisotropic atomic displacement parameters. Except for the hydrogen atoms of the methyl group C8 (refined with restriction on bond angles and bond angles), all other coordinates of hydrogen atoms were calculated.

Comments on the Crystal Structure of L8·3$CHCl_3$. All non-hydrogen atoms (74) were refined with anisotropic atomic displacement parameters. The hydrogen atoms were observed and refined with isotropic atomic displacement parameters. The maximum residual electronic density was located in the vicinty of the disordered chloroform molecule, while the two other solvent molecules did not show significant disorder.

Comments on the Crystal Structure of $[Lu_2(\mathbf{L7})_2](CF_3SO_3)_4](CF_3SO_3)_2 \cdot CH_3CN \cdot 3H_2O$ (6). The double-stranded cationic complexes $[Lu_2(\mathbf{L7})_2(CF_3SO_3)_4]^{2+}$ were arranged in polymer-like chains along the direction of their helical axis, via short contact interactions involving the two disordered ionic triflate anions. These chains were further packed into parallel planes and separated by large voids filled with highly disordered solvent molecules (Figure S16, Supporting Information). This mainly explained the very poor quality of the best diffraction data that we were able to obtain. We performed "SQUEEZE"[50]

(46) Altomare, A.; Burla, M. C.; Camalli, M.; Cascarano, G.; Giacovazzo, C.; Guagliardi, A.; Moliterni, G.; Polidori, G.; Spagna, R. *J. Appl. Crystallogr.* **1999**, *32*, 115.
(47) Sheldrick, G. M. *SHELXL97 Program for the Solution and Refinement of Crystal Structures*; University of Göttingen, Göttingen, Germany, **1997**.
(48) *XTAL 3.2 User's Manual*; Hall, S. R., Flack, H. D., Stewart, J. M., Eds.; Universities of Western Australia and Maryland, 1989.
(49) Johnson, C. K. *ORTEP II*; Report ORNL-5138, Oak Ridge National Laboratory, Oak Ridge, TN, **1976**.
(50) Van der Sluis, P.; Spek, A. L. *Acta Crystallogr.* **1990**, *A46*, 194–201.
(51) (a) Koper, G.; Borkovec, M. *J. Phys. Chem. B* **2001**, *105*, 6666–6674. (b) Koper, G. J. M.; van Duijvenbode, R. C.; Stam, D. P. W.; Steurle, U.; Borkovec, M. *Macromolecules* **2003**, *36*, 2500–2507. (c) Garcés, J. L.; Koper, G. J. M.; Borkovec, M. *J. Phys. Chem. B* **2006**, *110*, 10937–10950.

calculations, and the final refinements were performed using the resulting "solvent-free" F_o^2 data (details given in the associated CIF file). The residual disorder and the poor quality of the data were not compatible with deposition of this crystal structure in the CCDC database, but its importance for the ultimate confirmation of the global double-stranded helical structure adopted by the binuclear lanthanide complexes was crucial for this contribution. The 12 terminal ethyl groups were refined isotropically. Hydrogen atoms were calculated and constrained for bond lengths and bond angles. The triflate units were refined isotropically with restraints on bond lengths and bond angles, except for one triflate (S1TC1T) coordinated to Lu1, which was refined without restraints. One triflate, coordinated to Lu1, displayed positional disorder and was refined on two different sites (population parameters: PP = 0.47/0.53). The coordinated oxygen atoms of these triflate anions (O10P and O10T) were almost superimposed and did not distort the coordination polyhedra around Lu1. Two ionic triflates were located on special positions and were disordered about inversion centers, each accounting for 0.5 anion. The second ionic triflate showed quite large U_{iso} values, but attempts to refine it on different sites increased the number of refined parameters without significantly improving the quality of the fit. Three interstitial water molecules were found from the residual electronic density map, two of them displaying large U_{iso} values. We noticed the presence of one water molecule in the cavity inside the helical complex, located between the approximately parallel phenyl rings. The distances between encapsulated O_{water} and the two centroids of these phenyl ring centroïds were ~3.5 Å.

Acknowledgment. We thank Mr. P. Perrottet for carefully recording ESI-MS spectra, Mr. A. Pinto for recording ^{19}F NMR spectra, and Mr. P. Ryan for synthetic support. Financial support from the Swiss National Science Foundation is gratefully acknowledged.

Supporting Information Available: Geometric parameters and crystal data for the crystal structures of **S6**, **L8**·3CHCl$_3$, and [Lu$_2$(**L7**)$_2$](CF$_3$SO$_3$)$_4$](CF$_3$SO$_3$)$_2$·CH$_3$CN·3H$_2$O (**6**) (Tables S1, S2, S6, and S7, Figures S2, S3, and S16, and CIF files), ^{1}H NMR data (Tables S3 and S4 and Figures S4−S10), elemental analysis data (Table S5), experimental synthetic procedures for **S6** (Scheme S1) and for synthons **1** and **2** (Scheme 3), illustration of previous self-assemblies of unsaturated helicates (Figure S1) and representation of conformational isomers (Scheme S2), species distribution curves (Figures S11, S12, and S14) and statistical factors (Figure S13), and the thermodynamic self-assembly process of [Lu$_2$(**L8**)$_n$]$^{6+}$ (Figure S15). This material is available free of charge via the Internet at http://pubs.acs.org.

(52) (a) Borkovec, M.; Hamacek, J.; Piguet, C. *Dalton Trans.* **2004**, 4096–4105. (b) Dalla Favera, N.; Hamacek, J.; Borkovec, M.; Jeannerat, D.; Ercolani, G.; Piguet, C. *Inorg. Chem.* **2007**, *46*, 9312–9322.

(53) Piguet, C.; Bünzli, J.-C. G. In *Handbook on the Physics and Chemistry of Rare Earths*; Gschneidner, K. A., Jr., Bünzli, J.-C. G., Pecharsky, V. K., Eds.; Elsevier Science: Amsterdam, 2009; Vol. *40*, pp 301−553.